Copyright Warning & Restrictions

The copyright law of the United States (Title 17, United States Code) governs the making of photocopies or other reproductions of copyrighted material.

Under certain conditions specified in the law, libraries and archives are authorized to furnish a photocopy or other reproduction. One of these specified conditions is that the photocopy or reproduction is not to be "used for any purpose other than private study, scholarship, or research." If a, user makes a request for, or later uses, a photocopy or reproduction for purposes in excess of "fair use" that user may be liable for copyright infringement,

This institution reserves the right to refuse to accept a copying order if, in its judgment, fulfillment of the order would involve violation of copyright law.

Please Note: The author retains the copyright while the New Jersey Institute of Technology reserves the right to distribute this thesis or dissertation

Printing note: If you do not wish to print this page, then select "Pages from: first page # to: last page #" on the print dialog screen

ABSTRACT

EXPERIMENTAL STUDY OF BUBBLE RUPTURE DURING SHOCK-FLUID INTERACTION

by
Subhalakshmi Chandrasekaran

Head injuries are associated with exposure to high energy explosive detonation. There are four distinct types of blast induced neurotrauma (BINT): 1) these caused by supersonic shock waves propagating in the atmosphere (primary), 2) high velocity impact of shrapnel and debris (secondary) 3) acceleration and deceleration of the body and collision with the solid objects in the field (tertiary) and 4) exposure to high temperature and toxic gases (quaternary). One of the mechanisms implicated in non-impact primary blast-induced traumatic brain injury (bTBI) is cavitation. It is hypothesized that cavitation can occur in the cerebrospinal fluid (CSF) layer, brain interstitial fluid, and possibly also in the cerebral blood. In this thesis, it is tested that if a bubble is present, it collapses when a shock wave passes through it.

The effect of shock waves on cavitation is simulated using a fluid filled cylinder made of polycarbonate. This simplified model represents the idealized skull-brain complex and was subjected to blast with the Friedlander waveform type of loading. Bubbles are introduced in the fluid filled cylinder in a controlled manner and the behavior of these bubbles during the blast is studied using fluids with different properties at two discrete shock wave intensities.

It is found that the bubbles collapse under shock loading and partially regroup after the passage of the shock. The frequency of pressure wave in the fluid is altered during the collapse and regrouping.

EXPERIMENTAL STUDY OF BUBBLE RUPTURE DURING SHOCK-FLUID INTERACTION

by
Subhalakshmi Chandrasekaran

A Thesis
Submitted to the Faculty of
New Jersey Institute of Technology
in Partial Fulfillment of the Requirements for the Degree of
Master of Science in Biomedical Engineering

Department of Biomedical Engineering

May 2017

APPROVAL PAGE

EXPERIMENTAL STUDY OF BUBBLE RUPTURE DURING SHOCK-FLUID INTERACTION

Subhalakshmi Chandrasekaran

Dr. Namas Chandra, Thesis Advisor Professor of Biomedical Engineering, NJIT	Date
Dr. Bryan J. Pfister, Committee Member Associate Professor of Biomedical Engineering, NJIT	Date
Dr. Maciej Skotak, Committee Member Research Assistant Professor of Biomedical Engineering, NJIT	Date

BIOGRAPHICAL SKETCH

Author: Subhalakshmi Chandrasekaran

Degree: Master of Science

Date: May 2017

Undergraduate and Graduate Education:

- Master of Science in Biomedical Engineering,
  New Jersey Institute of Technology, Newark, NJ, 2017

- Bachelor of Technology in Biomedical Engineering,
  Sathyabama University, Chennai, India, 2015

Major: Biomedical Engineering

To mom and dad
Who gave all their love and support,
And encouraged me to go on every adventure,
especially this one.

ACKNOWLEDGMENT

My deep gratitude goes first to Dr. Namas Chandra, who expertly guided me through my graduate education. The accomplishment of this task would not have been possible without his valuable guidance. His words of encouragement have been constantly inspiring me in my research and personal life as well.

I am greatly thankful to Dr. Bryan Pfister and Dr. Maciej Skotak for taking out their valuable time and serving in my thesis committee.

I am also indebted to the Office of Naval Research for funding the research and supporting my graduate study.

I thank Dr. Maciej Skotak and Mr. Eren Alay for their efforts and support on my thesis and for conducting the blast experiments.

I would also like to thank my colleagues and friends at the Center for Injury Biomechanics, Materials and Medicine, Jose Rodriguez and Abdus Ali who helped me during the entire course of my study.

Finally, I would like to express my gratitude to my family and friends for motivating me, without whom it would not have been possible for me to successfully complete my master's thesis.

TABLE OF CONTENTS

TABLE OF CONTENTS
(continued)

LIST OF TABLES

LIST OF FIGURES

LIST OF FIGURES
(Continued)

LIST OF FIGURES
(Continued)

Figure **Page**

LIST OF FIGURES
(Continued)

LIST OF DEFINITIONS

CSF	Cerebrospinal Fluid
IED	Improvised Explosive Devices
PMHS	Post Mortem Human Subjects
TBI	Traumatic Brain Injury
bTBI	Blast induced Traumatic Brain Injury

CHAPTER 1

INTRODUCTION

1.1 Background Information

Improvised explosive device (IED) use has become more prevalent in the asymmetric warfare in recent conflicts in Afghanistan and Iraq and blast injuries have become more common among military personnel. In order to uncover mechanisms of blast induced neurotrauma (BINT), greater understanding of how shock waves interact with the human head is required.

Blast induced neurotrauma can be classified into four distinct types: 1. Primary:-- caused by supersonic shock waves propagating in the atmosphere, 2. Secondary:-- sharpnel or debris from the blast causing head injury, 3. Tertiary:-- head injury due to acceleration-deceleration and 4. Quaternary:-- caused due to exposure to toxic inhalants (Cernak and Noble-Haeusslein).

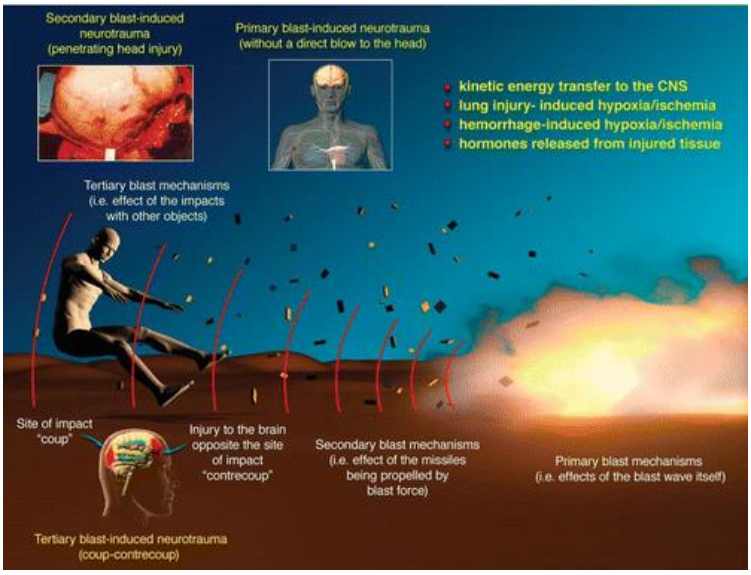

Figure 1.1 Different modes of BINT.
Source: (Cernak and Noble-Haeusslein)

Despite several years of research in the field of brain injury, it is still unclear as to how exactly the brain injury occurs and what are the mechanisms that cause the injury. Over the past few years, several mechanisms of blast-induced traumatic brain injury (bTBI) have been suggested: a) thoracic surge, b) translational and rotational head acceleration, c) direct transmission where blast wave passes through the cranium, d) skull flexure and e) cavitation.

More specifically, we will discuss cavitation as a possible damage mechanism causing traumatic brain injury (TBI). When a frontal blast wave encounters the head, a shock wave is transmitted through the skull, cerebrospinal fluid (CSF), and tissue, causing negative pressure at the countercoup that may result in cavitation (Goeller et al.).

Experiments to comprehensively study the interaction of shockwaves with animals and PMHS (Post Mortem Human Subjects) are often expensive and require ample time; this project proposes alternative means to study this phenomenon.

1.1.1 Shock Wave Theory

A blast wave is the pressure and flow resulting from the deposition of a large amount of energy in a small localized volume. In simpler terms, a blast wave is an area of pressure expanding supersonically outward from an explosive core (Neumann; and von). It has a leading shock front with microsecond rise time of compressed air. High-order explosives, when detonate, generate shock waves.

Shock waves have properties like any other waves, i.e. they can diffract through a narrow opening and refract as they pass through materials. Similar to sound waves, when the shock waves reach a boundary between two materials, part of it is transmitted, part of it is absorbed and a part of it is reflected. The impedances of the materials determine how

much of each occurs.

The simplest form of a shock wave has been described and termed as Friedlander waveform (J.M.Dewey). It occurs when a high explosive detonates in a free field, that is, with no surfaces nearby with which it can interact.

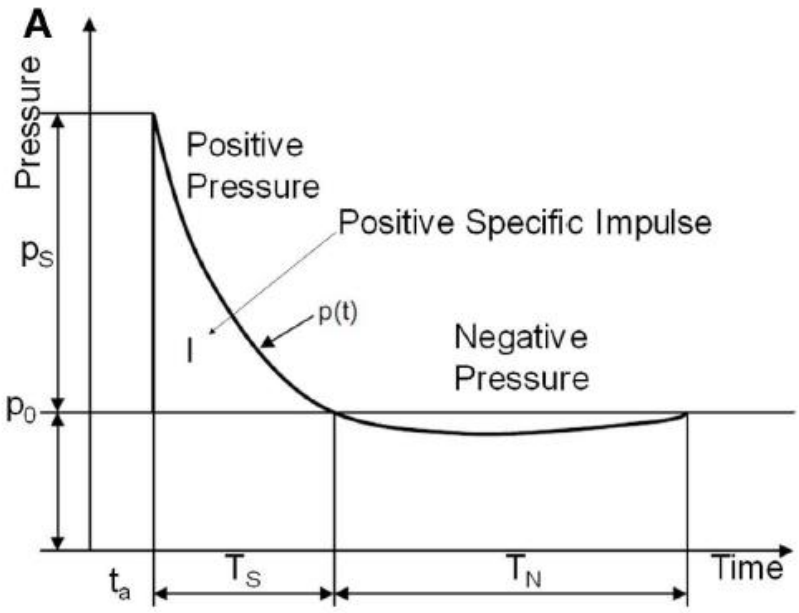

Figure 1.2 Friedlander waveform.
Source: (K.Gupta and Przekwas)

Consider:

$$\boldsymbol{p(t) = p_o\left(1 - \frac{t}{t_d}\right)e^{\left(\frac{-t}{\propto}\right)}}$$

Where p_0 is the blast over pressure, t_d is the positive time duration and α is the decay constant.

In a free field blast, the intensity of the shock wave will be gradually decreasing as it moves further and further away from the explosion epicenter. The pressure varies depending upon the elapsed time and propagation distance.

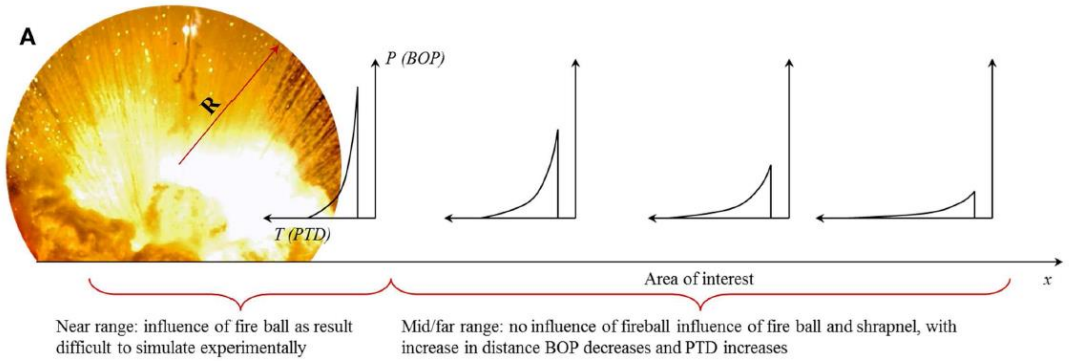

Figure 1.3 Blast wave profile decreasing with the increase of distance from exploded region.
Source: (Sundaramurthy and Chandra)

Achieving a Friedlander waveform in the laboratory conditions might vary from original free field conditions. The shock tube in Dr.Chandra's lab is able to generate pure shock loading conditions that closely mimic the field conditions.

1.1.2 Cavitation

Cavitation is defined as the process of formation and implosion of void (bubble) in a liquid which occurs in response to rapid change in pressure. In order to understand if cavitation is a valid mechanism of blast induced traumatic brain injury (bTBI), understanding when the bubbles form and collapse is critical.

Formation of bubbles in a liquid occurs when pressure drops below the vapor pressure at specific temperature. When pressure is restored, the bubbles collapse suddenly, producing a local shock wave that is capable of damaging nearby tissue and

structures. Cavitation is a common process and can be commonly seen as pitting in spinning boat propellers, demonstrating the potential for damage in softer materials such as brain (R.S.Salzar et al.).

Cavitation is often reported in lithotripsy techniques and in systems using phaco-emulsification probes or ultrasound waves (E.Brennen). Phacoemulsification probes are commonly used in ocular surgeries for breakdown of cataracts by vibrating at an ultrasonic frequency. Focused ultrasound, used in the destruction of kidney and gallbladder stones, was also reported to induce cavitation (E.Brennen).

In recent years computational models have demonstrated that high-rate impacts and blast waves can produce cavitation under the negative pressure occurring at the countercoup location. Macroscale simulations predict the possibility of cavitation at regions where the CSF and blood concentrations were the dominant part of the tissue composition (Haniff et al.). The collapse of such cavitation bubbles may contribute to the damage during the time head injury takes place.

Cavitation is also believed to occur in response to a high pressure shockwave, i.e when the tissue is compressed and then decompressed as the shock wave passes by. However, there are no literature reports which demonstrate the relationship between observed brain pathologies with this specific type of injury, specifically cavitation. Moreover, there are no existing methods which allow direct observation of cavitation as a result of interaction of a shock wave with human or animal brain. Thus, scientists frequently resort towards using surrogate models which, while sacrificing biofidelity, offer other advantages: simplified geometry and material transparency which allows video imaging in a controlled testing environment.

1.2 Objective

The primary objective of this project is to investigate how a shockwave interacts with bubbles generated in a fluid-filled cylinder. In this study the fluid-filled cylinder represents the skull-brain complex where the cylinder represents the skull and the fluid represents the components where probability of cavitation is the highest, i.e cerebrospinal fluid and blood.

An instrumented cylinder, with and without bubbles are exposed to blast loads at two incident pressures 70 and 130 kPa to study the effect of the shock wave with variations in the fluid composition inside the cylinder.

The main questions needed to be addressed are:

1. What effect does the type of fluid in the cylinder have on the bubbles disruption?
2. How does the introduction of bubbles affect the pressure inside of the fluid during shock wave passage?

CHAPTER 2

DEVICE REQUIREMENTS

In this chapter, we will explore the design of the blast wave facility and the experimental setup which is used to determine the interactions of the shockwave on a circular cylinder.

2.1 Shock Tube

The 9-inch square cross section shock tube is a facility where generated shock waves mimic closely the parameters of idealized real-life scenario with Friedlander type waveform. This shock tube consists of five main regions:

1. Driver Section (I)
2. Membrane Loading Deck
3. Driven Section (II,III)
4. Test Section Equipped with Observation Window
5. End Plate (IV)

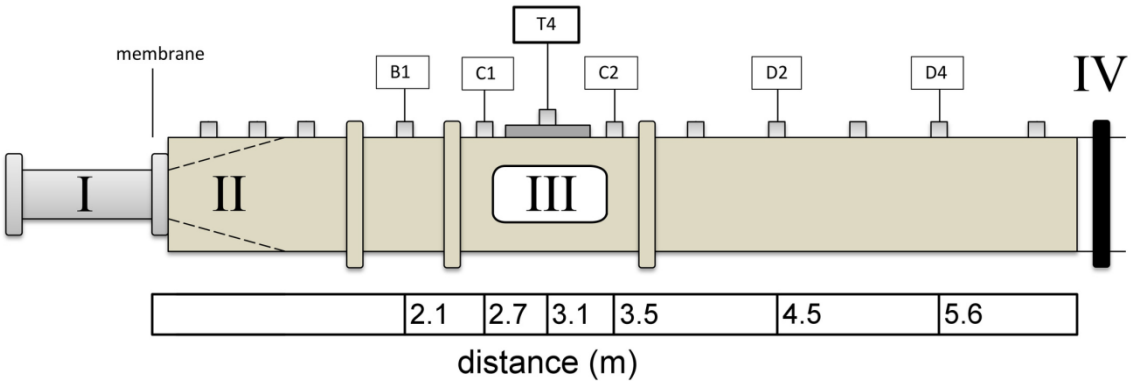

Figure 2.1 Shock tube schematic diagram.
Source: (Kuriakose et al.)

2.1.1 Driver Section

The driver section consists of a breech which is filled with different types of pressurized gases (helium, nitrogen or other based on the need). The driver section is connected to pressurized gas cylinders through pipes and is closed when not in use.

2.1.2 Membrane Loading Deck

This section of the shock tube determines the intensity of the shock wave. Mylar membranes of thickness 0.01" are used. Number of Mylar membranes depends on the desired intensity of the shock wave. The compressed driver gas ruptures the membranes creating the shock wave. Thus, by increasing the number of membranes, we increase the pressure required by the gas to rupture the membrane, also called as burst pressure.

2.1.3 Driven Section

This is the section of the shock tube where the shock wave propagates. It has 9" square cross section and 240" length and is made of 0.25" steel in order to withstand the pressure and reduce vibrations.

The PCB 134A24 series tourmaline pressure transducers are placed throughout the driven section at different locations (figure 2.1), in order to observe the propagation of the shock wave.

2.1.4 Observation Window

This section is essentially a part of the driven section where the specimen is placed under the shock loading conditions. A 0.75" thick, laminated polycarbonate called Lexgard® is used in this section to monitor specimen.

FASTCAM Mini UX100 camera is used to record the video footage through the

transparent glass window. It is a high speed camera for slow motion analysis and captures 720p High Definition video as fast as 6400 frames per second (fps) and reduced resolution all the way up to 800,000 fps.

2.1.5 End Plate

The end plate is typically used to control the extent of secondary waves or eliminate them completely making sure that the specimen is exposed only to a single shock wave with well-defined characteristics.

2.2 Polycarbonate Cylinder

A transparent polycarbonate cylinder with 7" height and 2" diameter with a uniform thickness of $1/16^{th}$ of an inch is used as representative of the skull in our simplified skull-brain model. Polycarbonate has been chosen as the representative of the skull as its acoustic impedance is close to that of the skull (Selvan et al.).

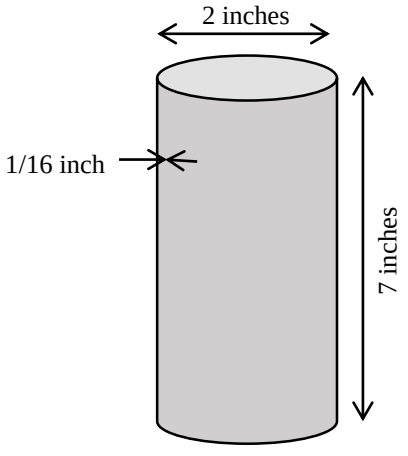

Figure 2.2 Polycarbonate cylinder with its characteristic dimensions.

Table 2.1 Material Properties
Source:(Selvan et al.)

Material	Density (kg/m^3)	Speed of sound (m/s)
Skull	1710	2900
Polycarbonate	1220	2270
Brain	1040	1509
Water	1000	1482

2.3 Fluid Media - Inside the Cylinder

Fluids of different viscosity are used in order to simulate different parts of the brain like the CSF, cerebral blood and the brain matter.

2.3.1 Viscosity Measurements

Experimental measurements of efflux time of glycerol-water solutions are done in the lab using Ostwald's viscometer and Cannon-Fenske viscometer. The Ostwald's viscometer is used for fluids with lower viscosity and Cannon-Fenske viscometer is used for fluids with higher viscosity. The relative dynamic viscosity is calculated using the formula:

$$\frac{\boldsymbol{\mu_1}}{\boldsymbol{\mu_0}} = \frac{\boldsymbol{t_1 * \rho_1}}{\boldsymbol{t_0 * \rho_0}}$$

Where, μ_1 is the dynamic viscosity of the fluid and t_1 and ρ_1 corresponds to the efflux time and the density of the fluid of interest. Similarly, μ_0, t_1 and ρ_1 correspond to deionized (DI) water.

Figure 2.3 Cannon-Fenske viscometer.
Source: Paragon scientific ltd

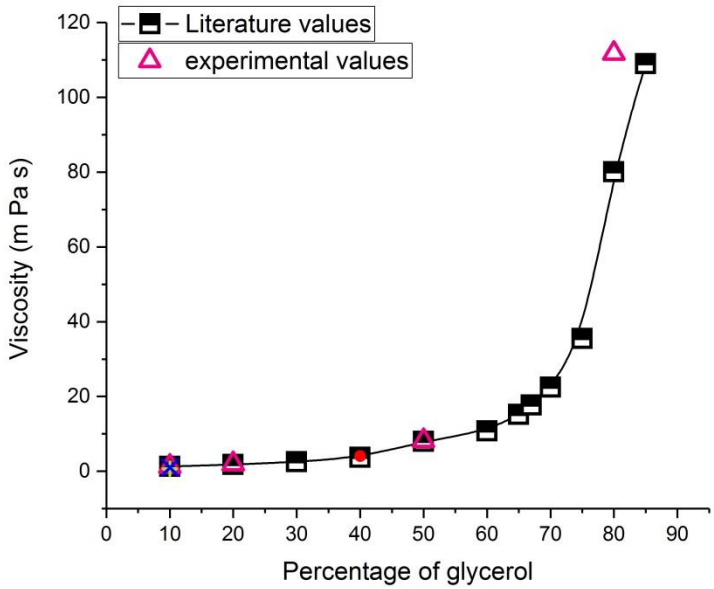

Figure 2.4 Viscosity measurements of glycerol-water solutions at room temperature.

Deionized (DI) water is used to simulate the CSF as the viscosity of these compounds closely matches.

Table 2.2 Viscosity of Glycerol-Water Solutions – Experimental and Theoretical Values

Solution	10% glycerol-water solution	20% glycerol-water solution	50% glycerol-water solution	80% glycerol-water solution
Experimental values (at room temperature)	1.312	1.944	8.194	111.998
Theoretical values at 20^{o} Celsius (Miner; and Dalton)	1.31	1.76	8.00	80.1

Viscosity of different solutions of glycerol are measured at room temperature and compared with the literature. Viscosity of 10%, 20%, 50% and 80% solutions of glycerol in water were measured. Viscosity of glycerol in water is not a linear function as shown in figure 2.4. The viscosity of 50% glycerol-water solution at room temperature was the closest to the viscosity of blood at body temperature (3 mPa.s) (Santner). Thus, 50% glycerol-water solution is used to simulate cerebral blood in our skull-brain model.

2.4 Kulite Sensors

The Kulite sensors (XCL-100 and XCEL-100) are used to measure the pressure changes inside the cylinder. These models are used as they are waterproof and are designed to operate in harsh environments. These are also ideal for use in most conductive liquids and gases. The pressure range of XCL-100 is from 0 to 50 psi and the pressure range of XCEL-100 is from 0 to 100 psi.

Figure 2.5 Kulite pressure sensor (XCL-100).
Source: Kulite XCL-100 data sheet

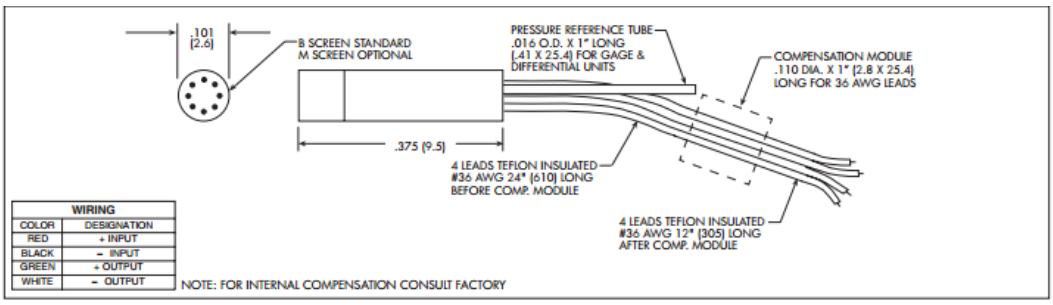

Figure 2.6 Dimensions and specifications of the sensor.
Source: Kulite XCL-100 data sheet

2.5 Surface Pressure Sensor

The LE-125 ultra-miniature pressure transducer is used to measure the surface pressure on the cylinder. They have a high natural frequency, extreme resistance to vibration and shock and hence are ideal to be mounted on the subject that has to undergo shock loading

conditions. The pressure range: 0 to 200 psi.

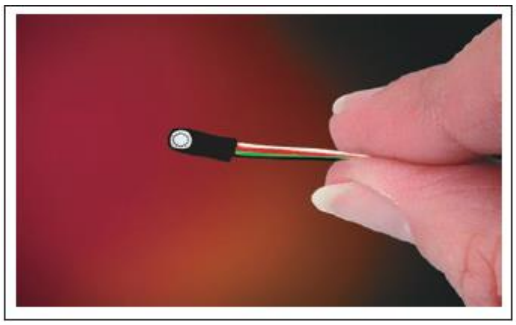

Figure 2.7 Kulite pressure sensor (LE-125).
Source: Kulite LE-125 data sheet

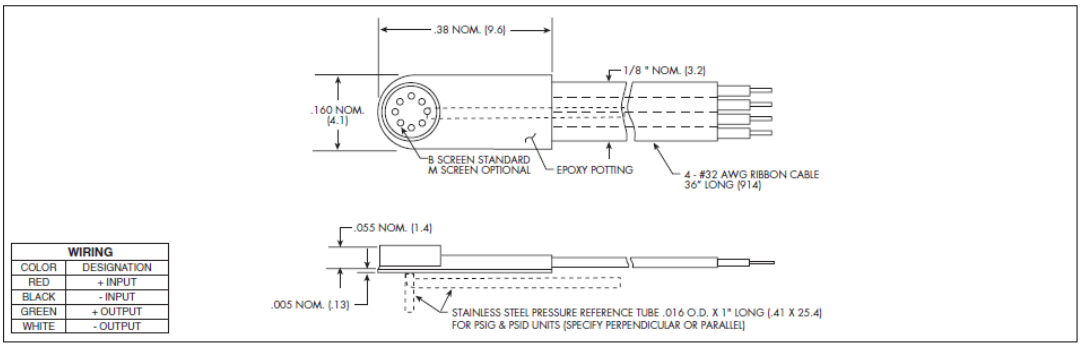

Figure 2.8 Dimensions and specifications of the sensor.
Source: Kulite LE-125 data sheet

2.6 Strain Gauges

Single-axis pre-wired strain gauges are used to measure the strain and the deformation of the cylinder under the shock loading conditions. They are pre-wired and hence soldering is not required. The strain gauge grids are as small as 10 mm and have a broad temperature range. The resistance of the strain gauge is 120.0 ± 0.8 Ω and the maximum excitation voltage is up to 14 volts.

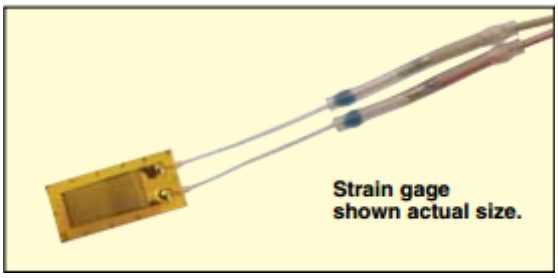

Figure 2.9 Pre-wired strain gauge.
Source: Omega pre-wired strain gauge data sheet

2.7 Cole-Parmer Syringe Pump

Syringe pumps can push out liquid through a syringe to obtain a known volume as determined by the size of the syringe. This syringe pump is used to pump air into the fluid-filled polycarbonate cylinder in order to produce the bubbles in a continuous and controlled manner.

Figure 2.10 Cole-Parmer single syringe infusion pump.
Source: Cole-Parmer data sheet

CHAPTER 3

EXPERIMENTAL METHODOLOGY

In this chapter, we discuss in detail the steps that were followed to conduct the experiments.

3.1 Cylinder Preparation

The polycarbonate cylinder is cut to size of 7 inches and it is made sure that it fits in the railings of the slider plates and into the test-section of the shock tube.

The slider plates are used to keep the cylinder inside the test section. These plates are made in such a way that we can choose to either fix the cylinder in one position (using screws) in the shock tube or let it move freely in one direction, parallel to the shock front (until a particular point). In our model, the cylinder is allowed to freely move when it is loaded.

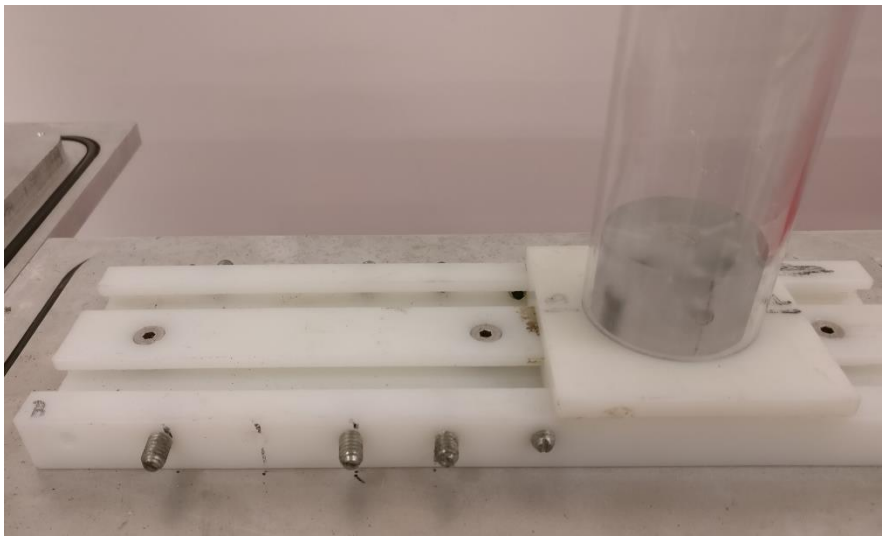

Figure 3.1 Slider plate with the cylinder placed on the grooves.

3.2 Cylinder Instrumentation

The polycarbonate cylinder is instrumented with two Kulite XCL-100 sensors to measure the pressure inside the fluid filled cylinder and one Kulite LE-125 surface mount sensor to measure the reflected pressure.

The desired position of the kulite XCL-100 is the middle of the cylinder. The length of the kulite metal lead is just 10 mm. It will not be possible to fix it inside the cylinder without any support. Thus the sensors are placed inside the cylinder by mounting them inside stainless steel tubing. This way, the wires are also protected inside the tubing. The sensors are mounted facing the shockwave at different positions as shown in the figure 3.2.

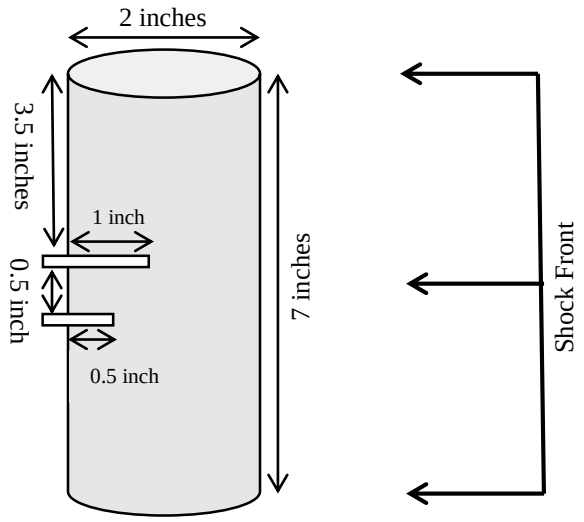

Figure 3.2 Polycarbonate cylinder with the position of pressure sensors.

Single-axis strain gauges are mounted on the three sides:- front, back and side of the cylinder, to measure the strain and the deformation of the cylinder under shock loading conditions.

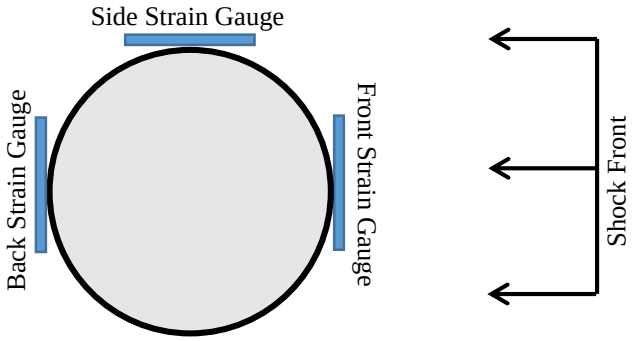

Figure 3.3 Top view of polycarbonate cylinder showing the position of the strain gauges.

Figure 3.4 Cylinder instrumented with pressure sensors and strain gauges.

3.3 Sealing the Cylinder

Since the fluid-filled cylinder is exposed to high pressure conditions, there is a high chance of leakage. A thin layer of ballistic gel is used to seal the bottom of the cylinder. 20% ballistic gel is used. The ballistic gel is clear at room temperature and it transforms

into a viscous fluid when heated, thickens in about 30 minutes and completely cures in 24 hours.

Sealing the top of the cylinder is one of the major issues as the cylinder should have enough opening for the bubbles to go. Initially, the cylinder was not completely filled with testy solution; a small gap was left for the bubbles to escape. Due to the gap, the liquid column moves vigorously during shock loading resulting in air incorporation into the liquid and interfering with the main purpose of the study. Thus, the cylinder was completely filled with the liquid and a hole was made on the top cap of the cylinder so that bubbles can escape through it.

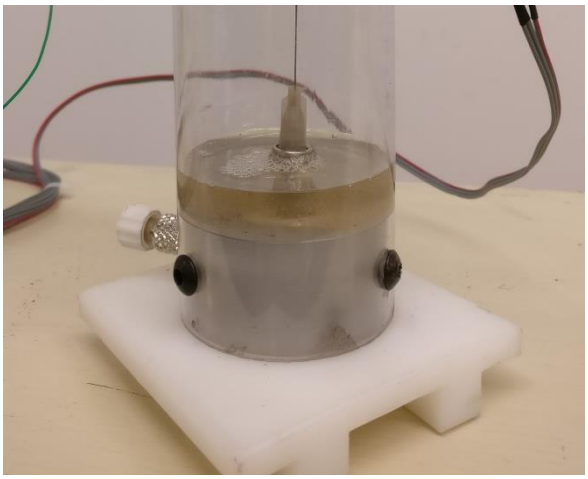

Figure 3.5 Sealing of the bottom of the cylinder with ballistic gel.

3.4 Generating Bubbles

The cap of the polycarbonate cylinder is drilled in the center in such a way that a Leur Lock female adapter can be attached which allows a needle of desired size to be placed on it. Also, the side of the cap is drilled to go all the way through, meeting the other hole in the center, which can be connected to the syringe on the Cole-Parmer syringe pump.

The syringe pump is used to push in air into the cylinder through a needle, using a syringe of 60 ml volume. The rate was fixed as 420 µl/min (which was the maximum rate possible using a 60 ml syringe) to achieve controlled and consistent bubbles.

Needles of different size are used in the experimental setup to generate bubbles and determine which needle provides the desired result.

An 18 Gauge needle produces 3 bubbles at an average interval of about 0.078 seconds (38.46 bubbles per second) with the fourth bubble produced at an average of 0.83 seconds.

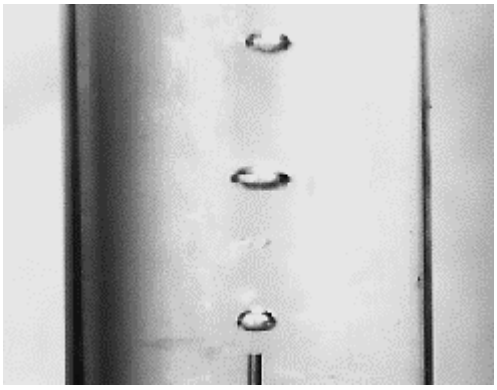

Figure 3.6 Bubbles generated by 18 Gauge needle.

A 21 Gauge needle produces 2 bubbles at an average interval of about 0.022 seconds and the third bubble is produced at an average of 0.318 seconds.

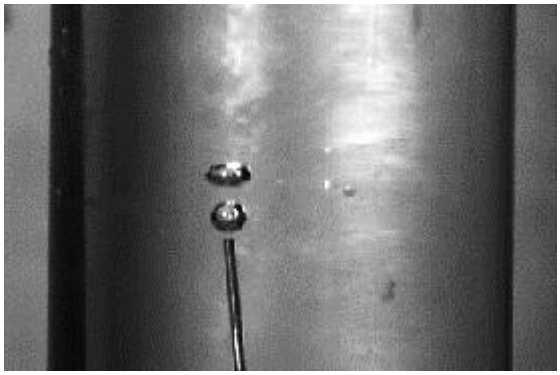

Figure 3.7 Bubbles generated by 21 Gauge needle.

A 22 Gauge needle is used to generate bubbles in the polycarbonate cylinder. 7 bubbles are generated continuously, each with an average interval of 0.028 seconds. A stream of 7 bubbles is produced with an interval that lasts for about 0.666 seconds on an average.

Figure 3.8 Bubbles generated by 22 Gauge needle.

The bubbles produced by the needles of different sizes mentioned above (18-22 G) were not desirable. The stream of bubbles was unsteady, i.e short burst of a few bubbles followed by a long pause and this flow pattern was repeated. Since we can't control precisely when the shock wave is initiated; constant, uninterrupted stream of bubbles is preferred, to increase chances of capturing bubble disruption next to the pressure sensor.

Only when a 23 Gauge needle was used to generate the bubbles in the experimental setup, continuous stream of bubbles was created with an average interval of 0.059 seconds per bubble. This was a desirable condition. Thus, 23 Gauge was chosen to be used.

Figure 3.9 Continuous stream of individual separated bubbles generated by 23 Gauge needle.

During the optimization stage of the experimental setup, the 23 Gauge needle was cut shorter so that more number of bubbles could be seen in the given volume of the cylinder. However, due to needle tip alteration caused by cutting, we couldn't generate bubbles in a consistent manner. A burst of 10 bubbles was produced each within an average interval of 0.059 seconds. The same pattern was repeated with an interval of 1.176 seconds.

Figure 3.10 Bubbles generated by 23 Gauge needle after cutting.

When the diameter of the needle was getting smaller, the bubbles were generated in a controlled, continuous and repeatable manner. Also, the size of the bubbles was visibly smaller as the size of the needle kept getting smaller. The smaller the bubbles, the better it is for the experiment, as it is closer to realistic conditions.

We found that the needle with a 27 Gauge gives the optimal stream of bubbles and it was chosen to generate the bubbles in the polycarbonate cylinder during shock wave exposure. The results were much better compared to needles with larger diameters. The generation of bubble was repeatable and continuous. The flow rate in the syringe pump was 423µl/min and a 60 ml syringe was used to pump ambient air through it.

Figure 3.11 Generation of bubbles in 50% glycerol-water solution using 27G needle.

3.5 Experimental Setup

The polycarbonate cylinder is tested outside the shock tube for consistent bubbles and is checked for any possible leaks. The cylinder is also sealed using silicone gel from the

outside to avoid any leaks.

The wires of the Kulite pressure sensors coming out from the stainless steel tubing are protected using quick-sil rubber so that the wires don't get damaged and there is no noise due to the extensive vibration of the wires when they are loaded under the shock loading conditions.

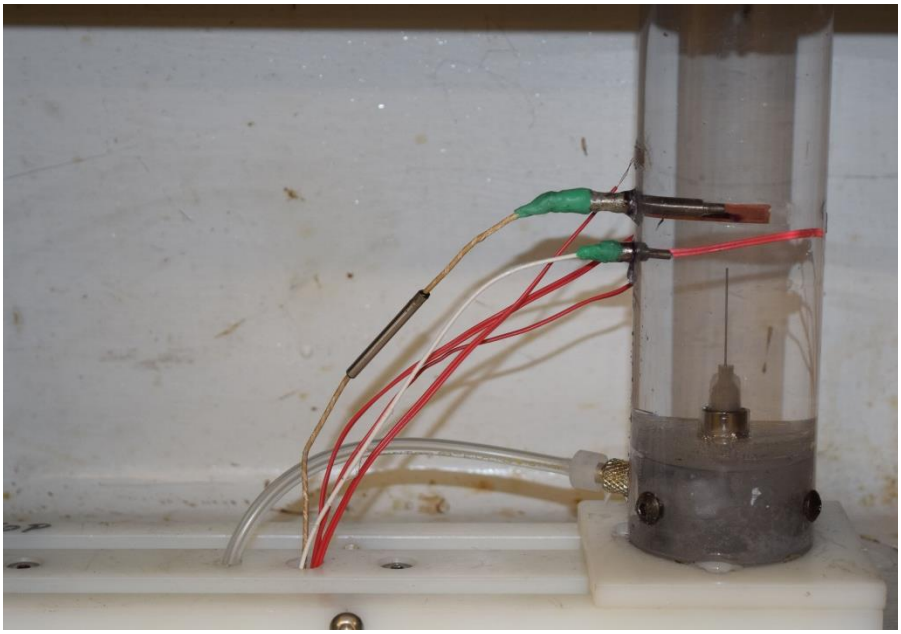

Figure 3.12 Experimental setup of the cylinder inside the shock tube.

CHAPTER 4

RESULTS AND DISCUSSION

When a shockwave interacts with the cylinder, we see a) the oscillations of the cylinder walls caused by shock wave impact and b) pressure wave which is transmitted to the fluid from the polycarbonate wall. The readings from the sensors and strain gauges are discussed in this chapter.

4.1 Cylinder Exposure to Shock Wave

The instrumented polycarbonate cylinder is exposed under shock loading conditions with and without bubbles in order to compare the two. The sensor is mounted in the middle of the cylinder at 3.5 inches height so that the tip is positioned 1 inch inside the cylinder i.e in the center of the cylinder, so that the pressure profiles during the bubble collapse can be measured in that location.

The polycarbonate cylinder is exposed to a shock wave at two different intensities:- 70 kPa and 130 kPa. DI water has been used as idealized CSF and 50% glycerol has been used as representative for cerebral blood.

Thus, the polycarbonate cylinder is exposed to the shock wave with two different media where each medium is exposed under two different conditions – with bubbles and without bubbles flowing upwards the cylinder. Bubbles in the cylinder are dispersed by shock wave to evaluate if bubbles have any effect on the recorded pressure profiles. The cylinder is allowed to move in X direction, parallel to the shock wave. An endpoint is set in the slider plates using screws and the cylinder is allowed to move only up to this point

when it is exposed to the shock wave.

Table 4.1 Cylinder Exposed to Shock Wave under Different Conditions

Nominal shock wave intensity	Medium inside the cylinder	Loading conditions	Number of repetitions
70 kPa	DI water	Without bubbles	4
		With bubbles	4
	50% glycerol-water solution	Without bubbles	4
		With bubbles	4
130 kPa	DI water	Without bubbles	4
		With bubbles	4
	50% glycerol-water solution	Without bubbles	4
		With bubbles	4
		Total	32

Table 4.1 shows the number of experiments done under different conditions. Number of repetitions was 4 for each condition.

4.2 Cylinder Exposed at 70 kPa

The polycarbonate cylinder is exposed to the shock wave at nominal peak overpressure 70 kPa and figures presented below illustrate the behavior of bubbles when exposed to shock wave.

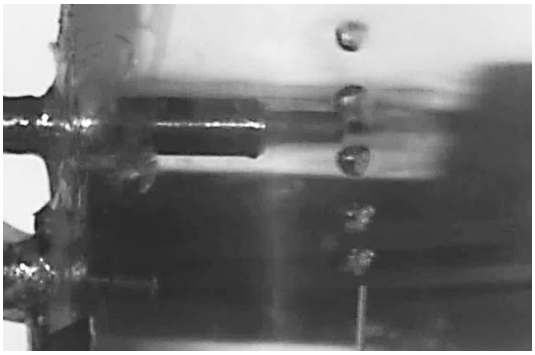

Figure 4.1 Air bubbles in 50% glycerol-water solution- 7 ms after the trigger.

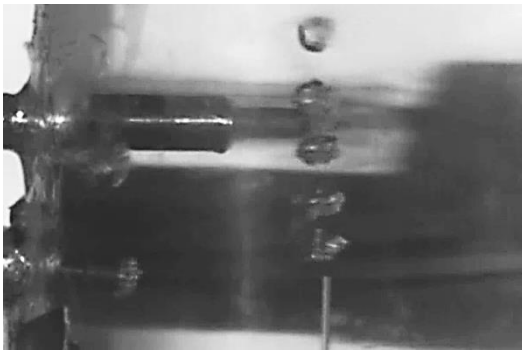

Figure 4.2 Air bubbles in 50% glycerol-water solution- 7.6 ms after the trigger.

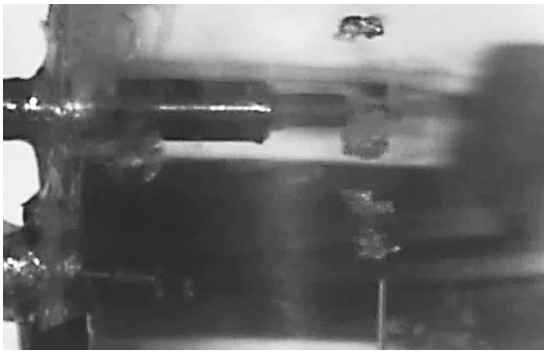

Figure 4.3 Air bubbles in 50% glycerol-water solution- 8.6 ms after the trigger.

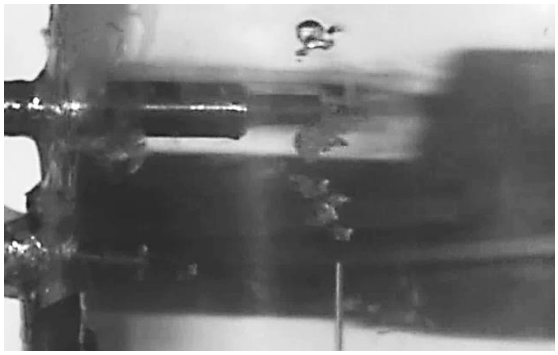

Figure 4.4 Air bubbles in 50% glycerol-water solution- 9.6 ms after the trigger.

Figure 4.5 Air bubbles in 50% glycerol-water solution- 10.2 ms after the trigger.

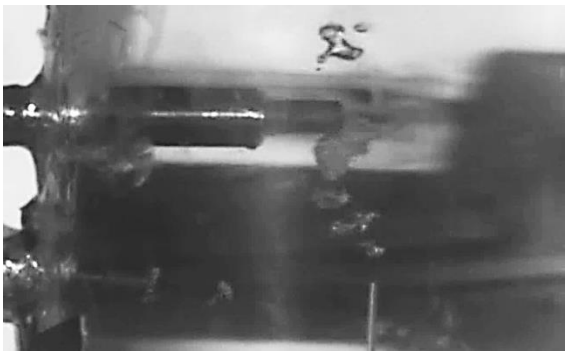

Figure 4.6 Air bubbles in 50% glycerol-water solution, 10.6 ms after the trigger.

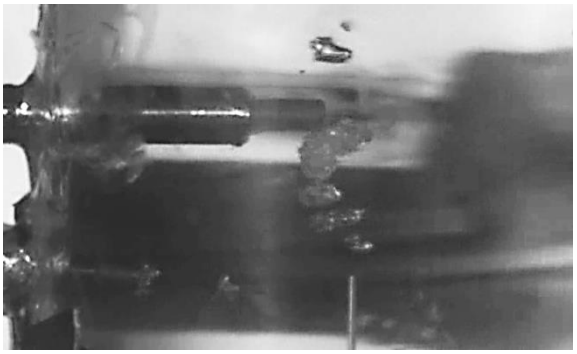

Figure 4.7 Air bubbles in 50% glycerol-water solution- 11.6 ms after the trigger.

Figure 4.8 Air bubbles in 50% glycerol-water solution- 36.6 ms after the trigger.

In figures 4.2 to 4.5, we can observe that the bubbles disperse into multiple smaller bubbles after exposure to the shock wave. In figures 4.6 to 4.8, the bubbles try to regroup after the shock wave has passed through.

4.2.1 Comparison of Pressure Profiles Inside the Fluids

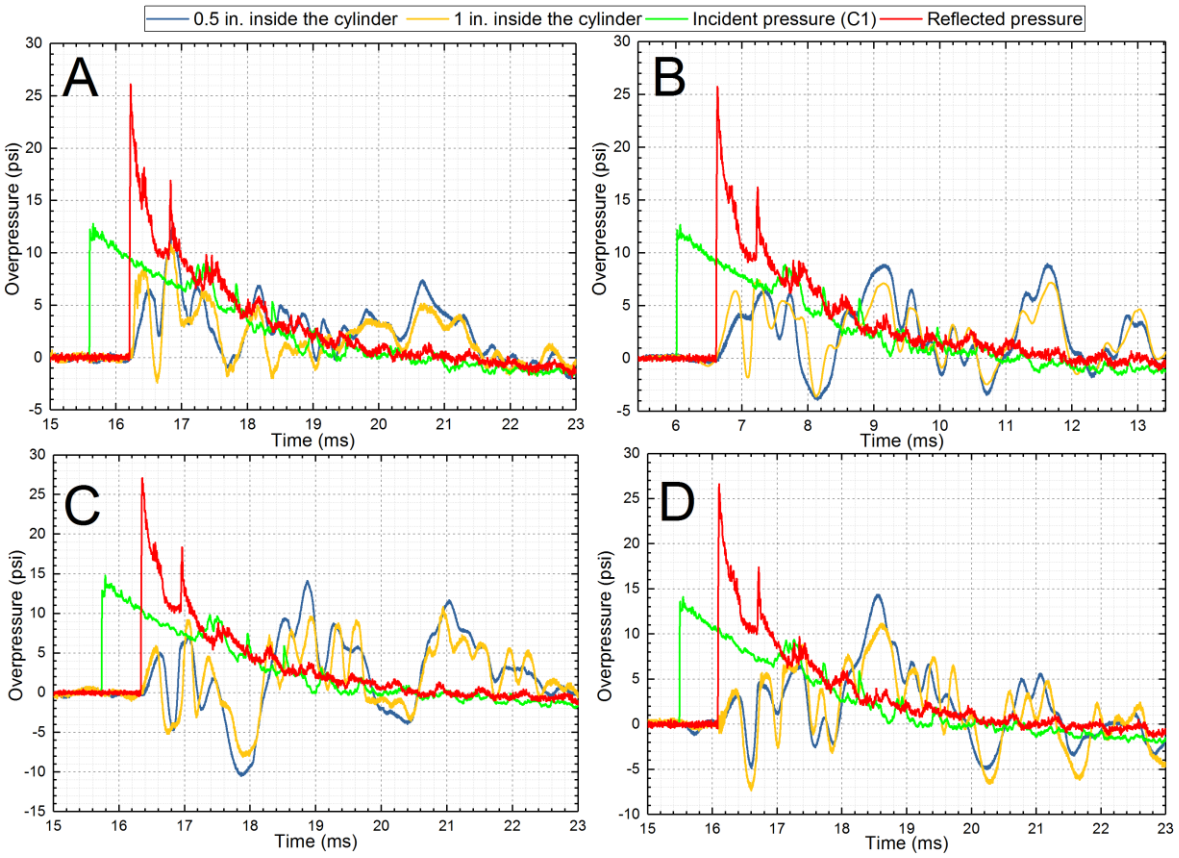

Figure 4.9 Incident, reflected and fluid pressure-time profiles recorded in four cases.
Note: The figure represents the pressure profiles in:

A. DI water without bubbles B. 50 % Glycerol solution without bubbles
C. DI water with bubbles D. 50% Glycerol solution with bubbles

In case C and D, higher peaks and more negative pressure is seen. This is due to the collapse of bubbles in the fluid. This indicates the change in pressure recorded by the pressure sensors with and without bubbles.

Fast Fourier transform was performed on the pressure profiles for better analysis of the raw data obtained from the pressure sensors. Since Fourier transform converts the data from time domain to frequency domain- possible effects associated with the presence of bubbles can be visualized by inspecting the spectra recorded at the same shock wave intensity in the same fluid with and without bubbles using a single sensor mounted in the specific location.

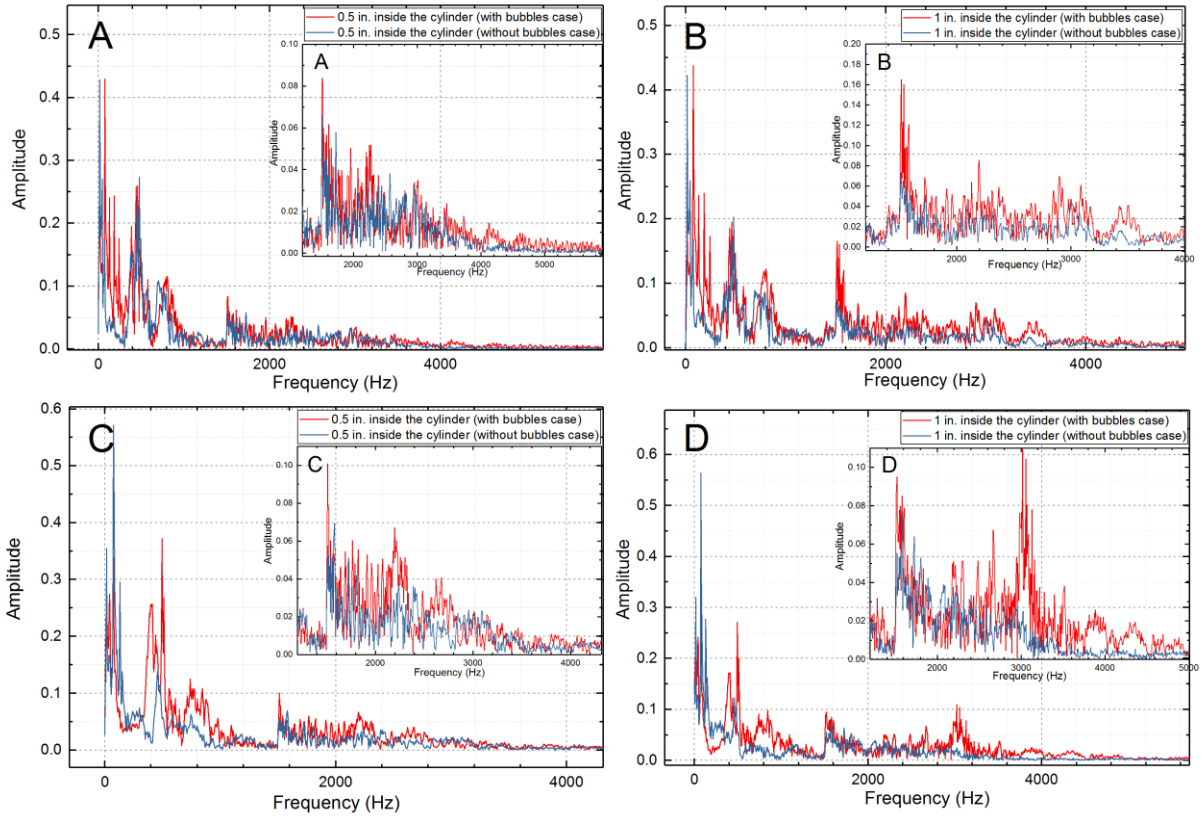

Figure 4.10 Fast Fourier transform analysis performed on pressure profiles recorded by sensors in different cases.

Note: The figure represents the comparison of the frequency response of the pressure profiles from the top and the bottom sensors with and without bubbles:

A. Bottom sensor in DI water
B. Top sensor in DI water
C. Bottom sensor in 50% glycerol solution
D. Top sensor in 50% glycerol solution

The top sensor in both fluids- DI water and 50% glycerol-water solution has higher amplitude at higher frequency in case where the bubbles were present during the shock loading conditions, which might indicate the bubble collapse has indeed a positive effect on the observed pressure.

To investigate the effect of bubbles on the pressure inside of the cylinder, we quamtified the peak overpressures recorded by the sensors in different cases. It was found that there was a higher variation in the peak overpressure in the top sensor, i.e the sensor which was the closest in contact with bubbles. This variation could be the due to the presence of bubbles and bubble rupture during the shock loading conditions.

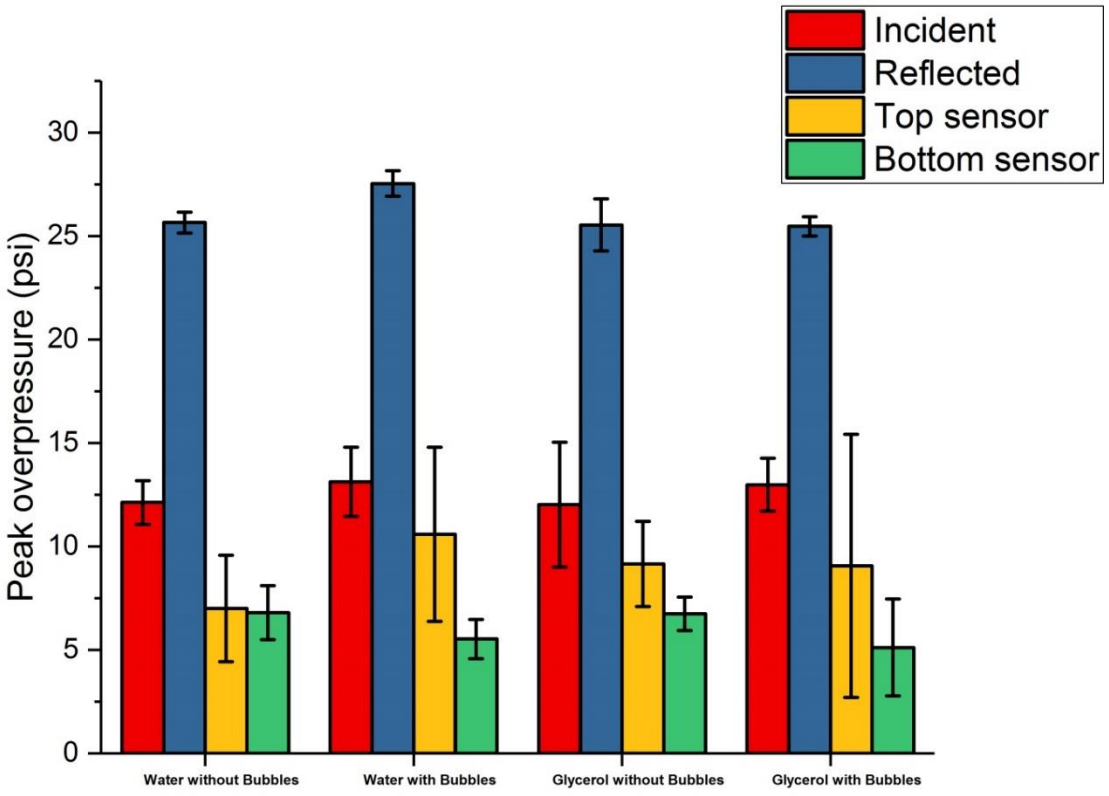

Figure 4.11 Comparison of peak overpressure values recorded by four sensors in different cases at 70 kPa nominal shock wave intensity.

4.2.2 Response of Strain Gauge in Different Cases

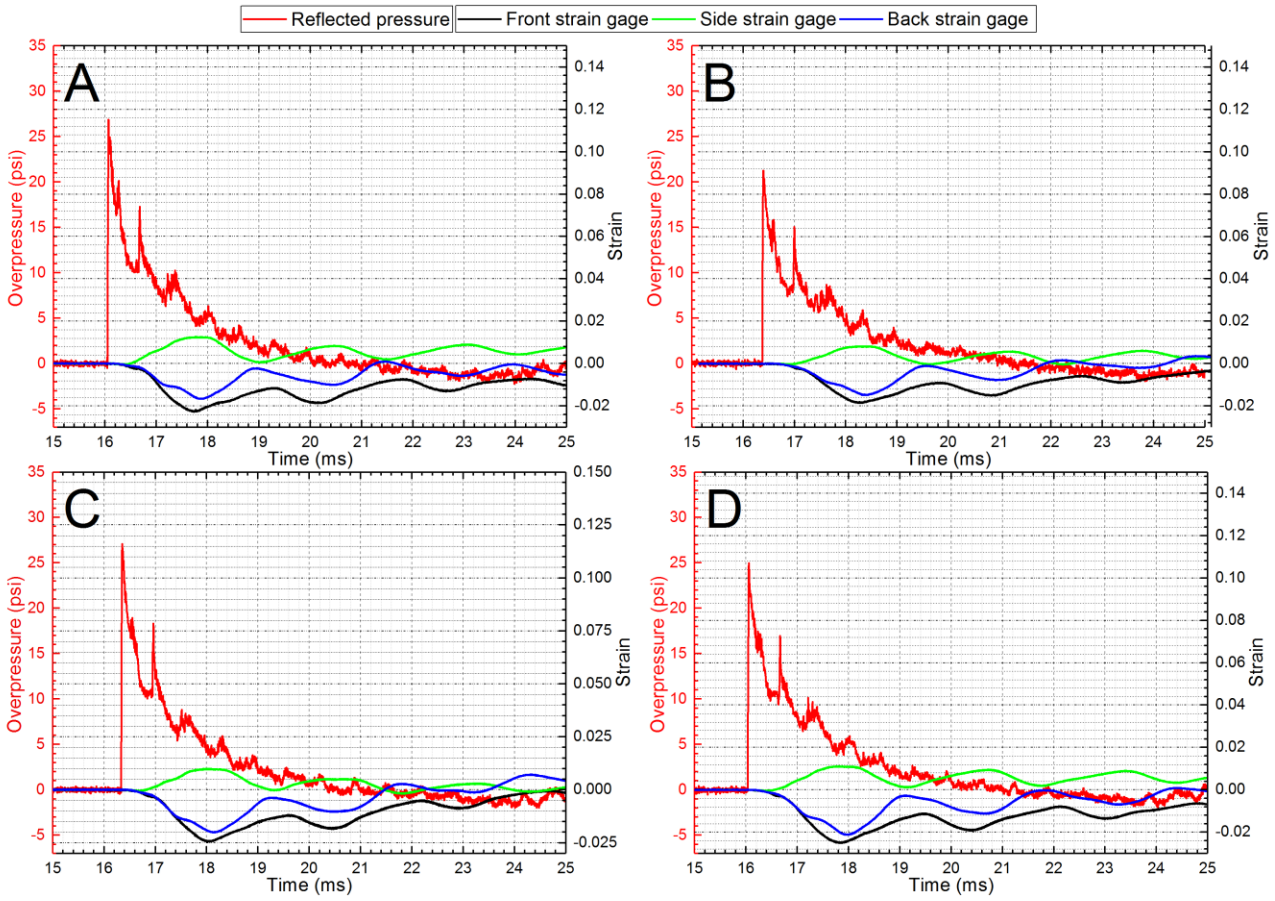

Figure 4.12 Time profiles of the strain gauges representing the tension and compression of the polycarbonate cylinder.

Note: The figure represents comparison of the strain gauge data during different cases:

A. DI water without bubbles B. 50% glycerol solution without bubbles

C. DI water with bubbles D. 50% glycerol solution with bubbles

The strain gauges measure the tension and compression of the cylinder walls when the cylinder is impacted by the shock wave. The strain gauge signal might be affected by the type of medium and the signal is correlated with the pressure inside of the cylinder.

Fast Fourier transform is performed for the strain gauge response to identify if there are any characteristic frequencies.

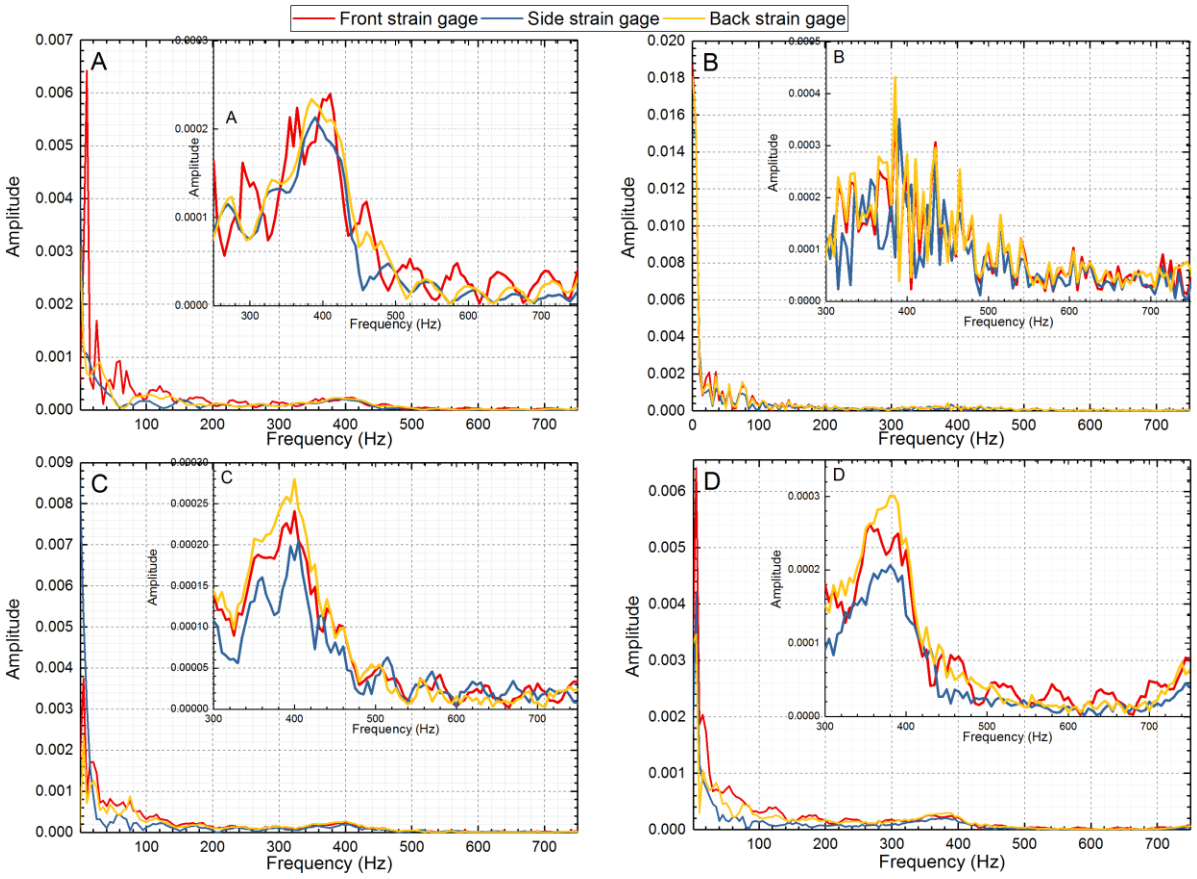

Figure 4.13 FFT of strain gauge signals recorded during different cases.

Note: The figure shows the comparison of the FFT of the strain gauge data under different conditions:

A. DI water without bubbles B. 50% glycerol solution without bubbles

C. DI water with bubbles D. 50% glycerol solution with bubbles

The Fourier transform of the strain gauge signals do not show any drastic change comparing the different cases, with a very distinct band at 300-500 Hz with peak around 400 Hz.

The arrival times of the strain gauges are also compared. It is seen that the side strain gauge lags substantially and the response of the front and back strain gauge is close to each other.

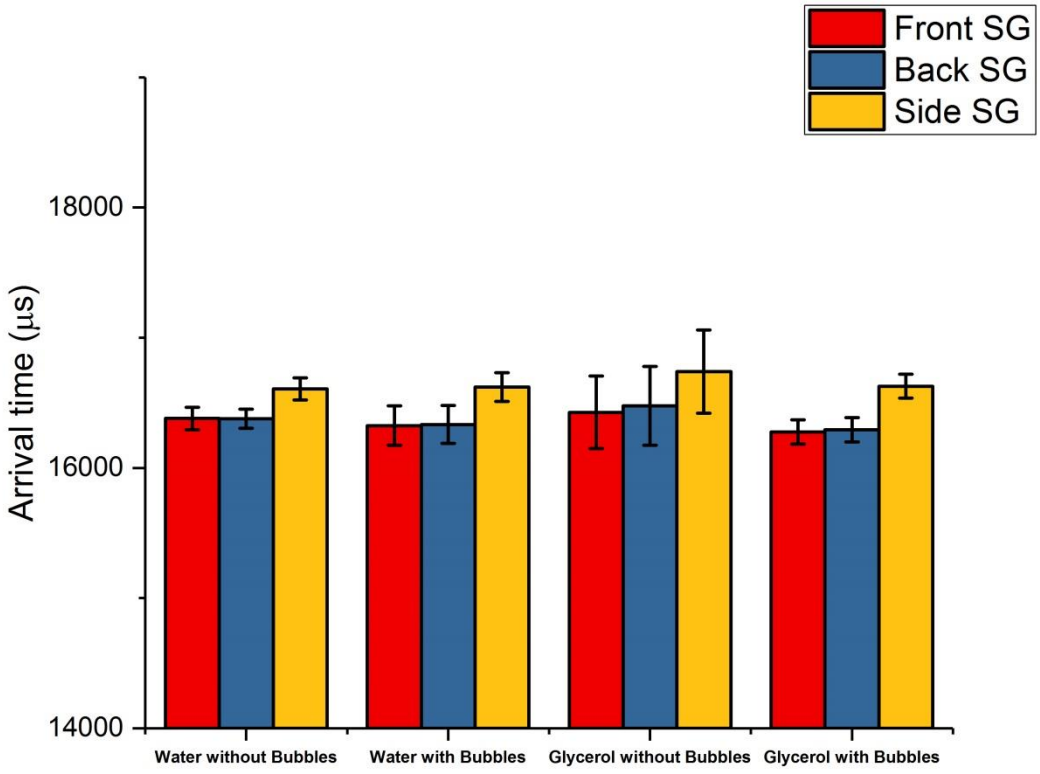

Figure 4.14 Comparison of arrival times for strain gauges at different locations.

Side strain gauge is lagging behind the front and the back strain gauge signals in all the cases independent of the medium present in the polycarbonate cylinder.

4.3 Cylinder Exposed at 130 kPa

The instrumented polycarbonate cylinder is exposed to 130 kPa and the collapse of bubbles is observed and changes and analyzed and quantified.

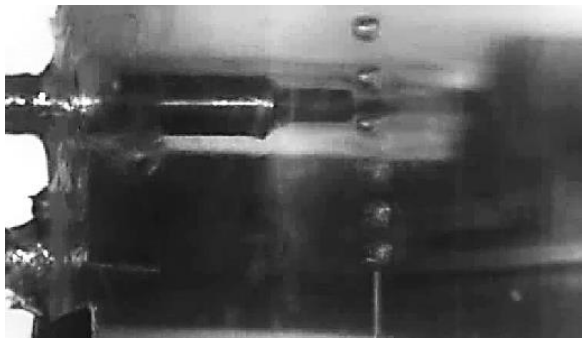

Figure 4.15 Air bubbles in 50% glycerol-water solution- 5.3 ms after the trigger.

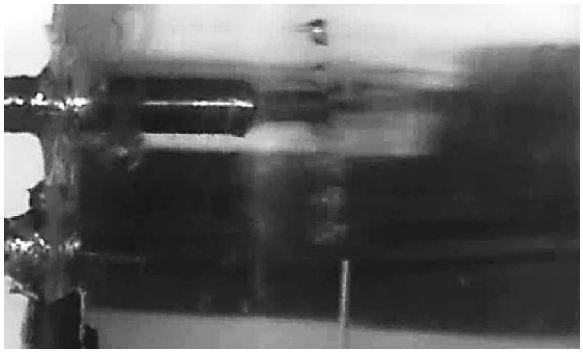

Figure 4.16 Air bubbles in 50% glycerol-water solution- 5.8 ms after the trigger.

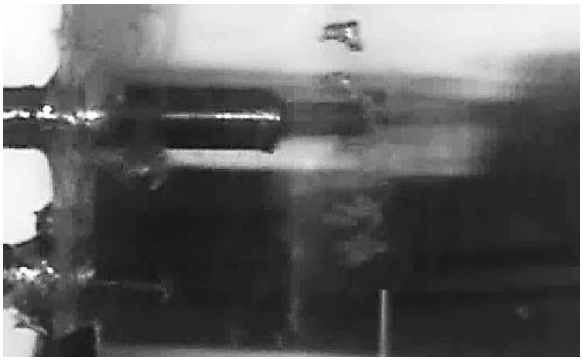

Figure 4.17 Air bubbles in 50% glycerol-water solution- 6 ms after the trigger.

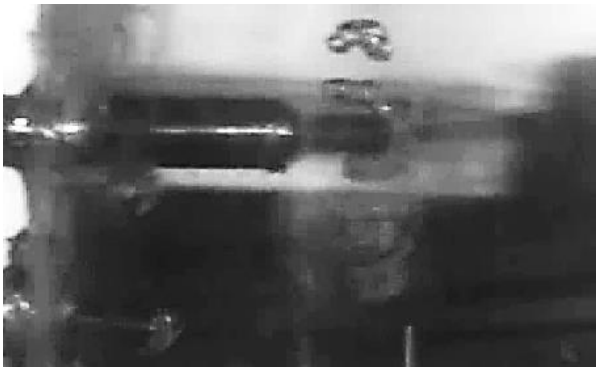

Figure 4.18 Air bubbles in 50% glycerol-water solution- 6.4 ms after the trigger.

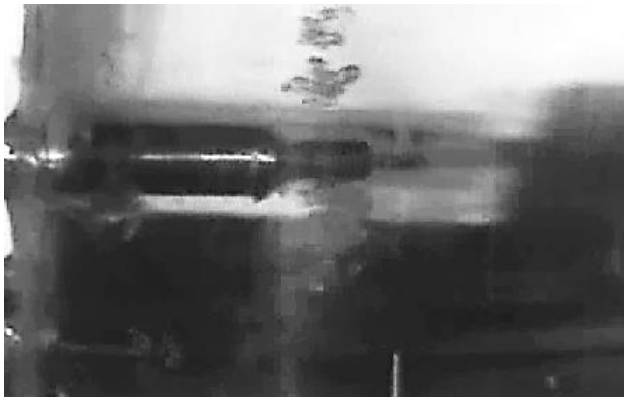

Figure 4.19 Air bubbles in 50% glycerol-water solution- 8.3 ms after the trigger.

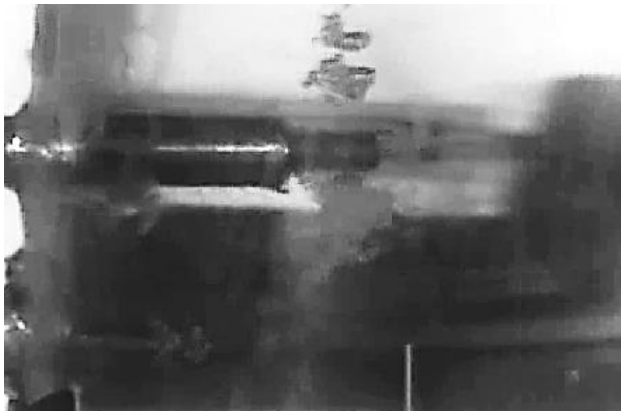

Figure 4.20 Air bubbles in 50% glycerol-water solution- 10.4 ms after the trigger.

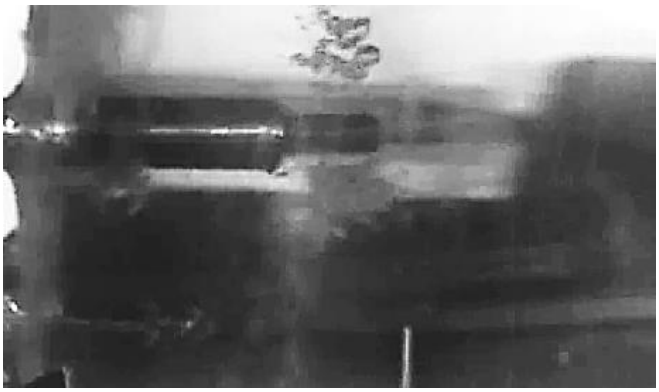

Figure 4.21 Air bubbles in 50% glycerol-water solution- 18.4 ms after the trigger.

Figure 4.22 Air bubbles in 50% glycerol-water solution- 25.4 ms after the trigger.

It is observed from figures 4.15 to 4.19 that the bubbles disperse into multiple smaller bubbles after exposure to the shock wave. In figures 4.20 to 4.22, the bubbles try to regroup after the shock wave has passed through**.**

4.3.1 Comparison of Pressure Profiles Inside the Fluids

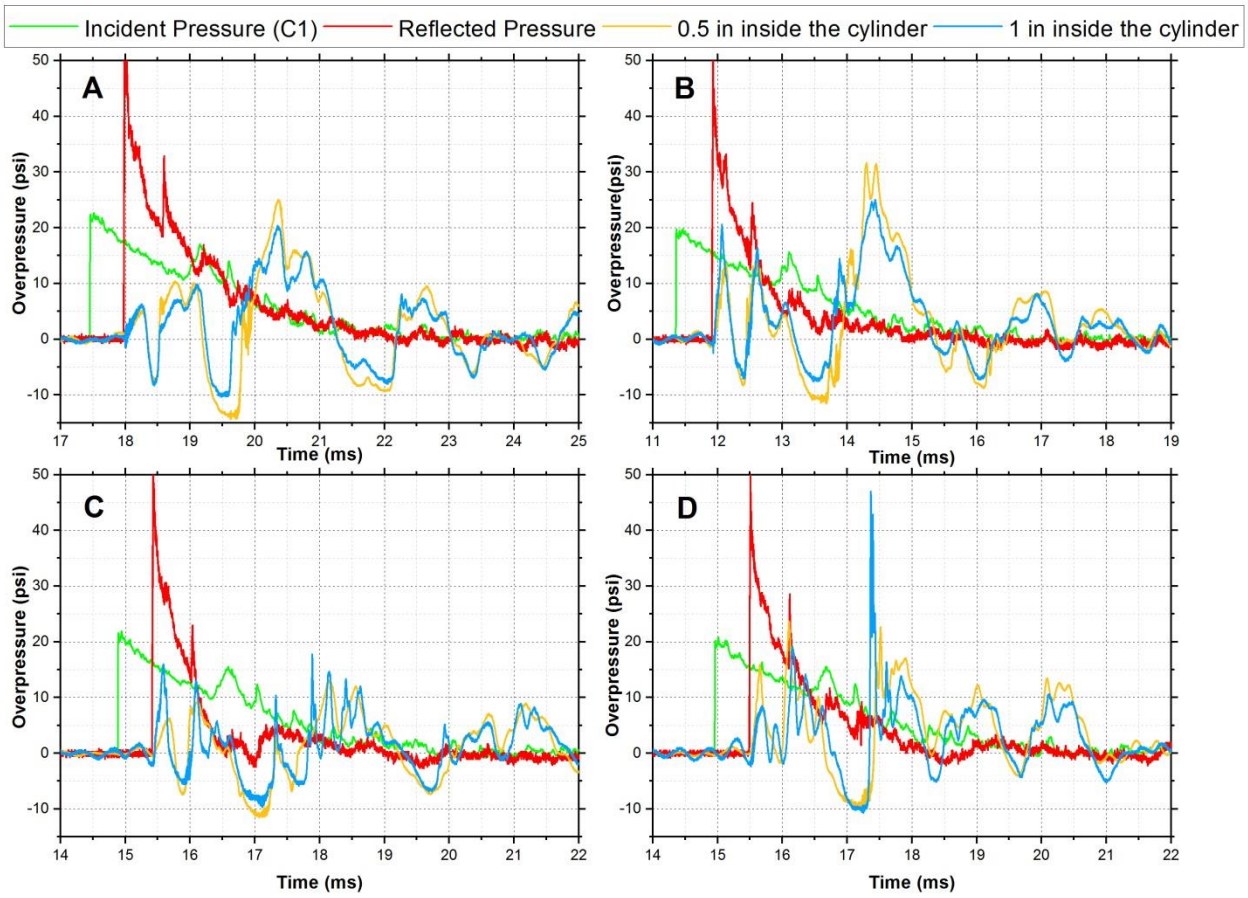

Figure 4.23 Incident, reflected and fluid pressure-time profiles recorded in four cases.
Note: The figure represents the pressure profiles in:

A. DI water without bubbles B. 50 % Glycerol solution without bubbles
C. DI water with bubbles D. 50% Glycerol solution with bubbles

In case C and D, more negative pressure is seen. This is due to the collapse of bubbles in the fluid. This indicates the change in pressure recorded by the pressure sensors with and without bubbles.

Fast Fourier transform was performed on the pressure profiles for better analysis of the raw data from the pressure sensors. Since Fourier transform converts the data from time domain to frequency domain, peaks in higher frequency would represent bubble rupture.

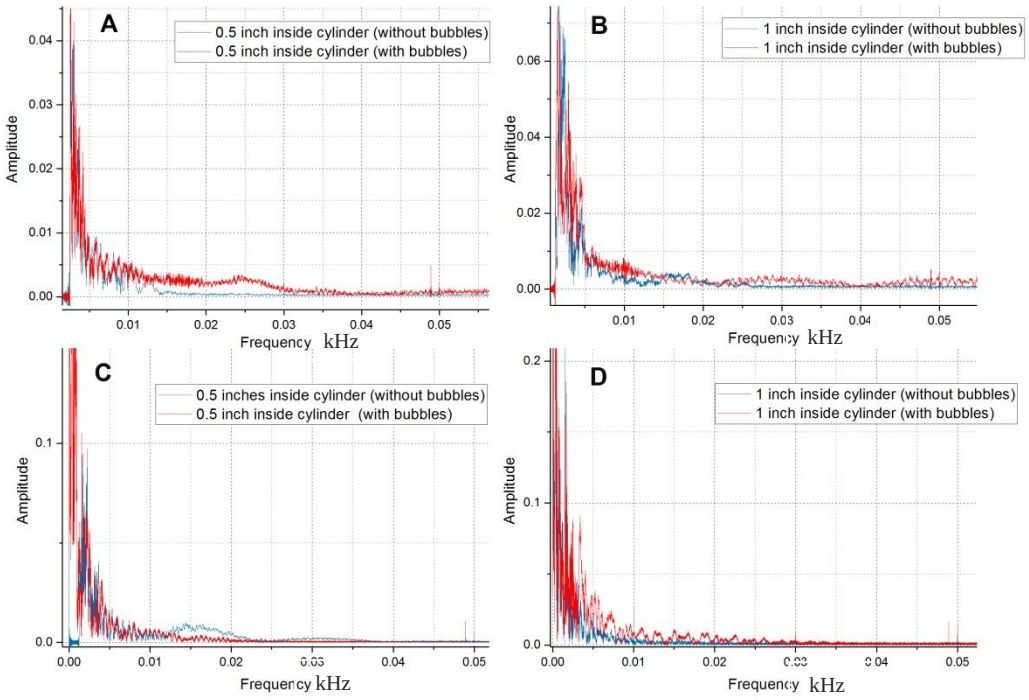

Figure 4.24 Fast Fourier transform analysis performed on pressure profiles recorded by sensors in different cases.

Note: The figure represents the comparison of the frequency response of the pressure profiles from the top and the bottom sensors with and without bubbles:

A. Bottom sensor in DI water
B. Top sensor in DI water
C. Bottom sensor in 50% glycerol solution
D. Top sensor in 50% glycerol solution

The top sensor in both the fluids has higher amplitude in higher frequency regions which represents bubble.

The peak overpressures of the sensors in different cases was quantified (figure 4.25). It was found that there was a higher variation in the peak overpressures in 50% glycerol-water solution (standard deviation of 16.35). This variation could be the due to the presence of bubbles and bubble rupture during the shock loading conditions.

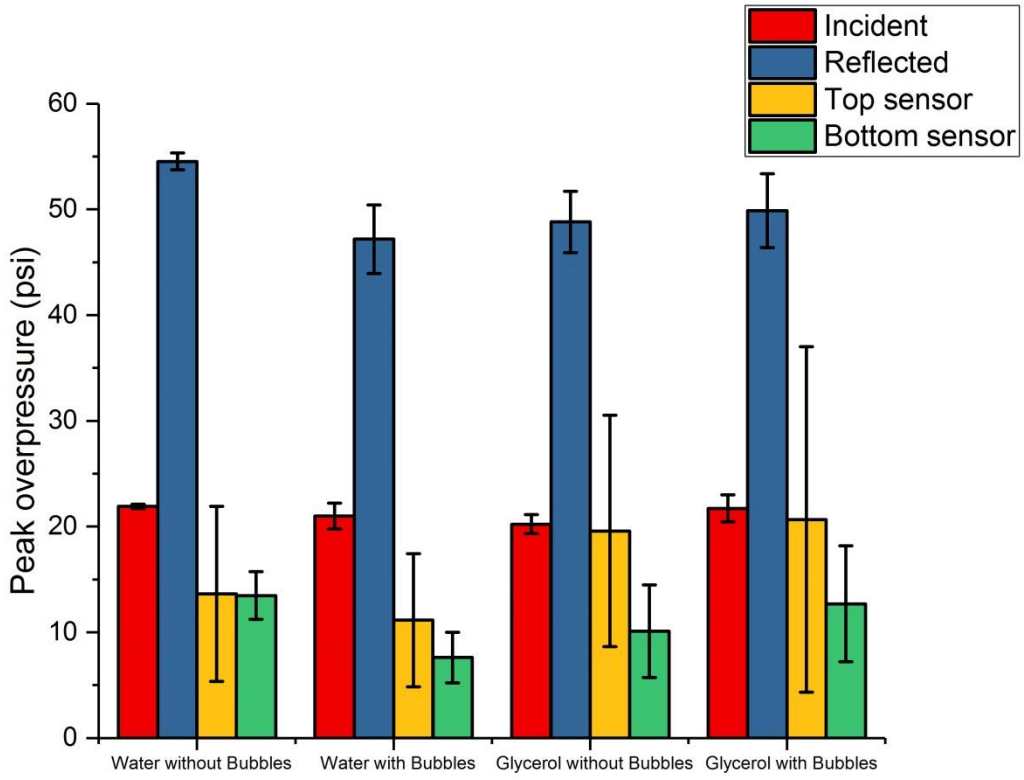

Figure 4.25 Comparison of peak overpressure values recorded by four sensors in different cases at 130 kPa nominal shock wave intensity.

4.3.2 Response of Strain Gauge in Different Cases

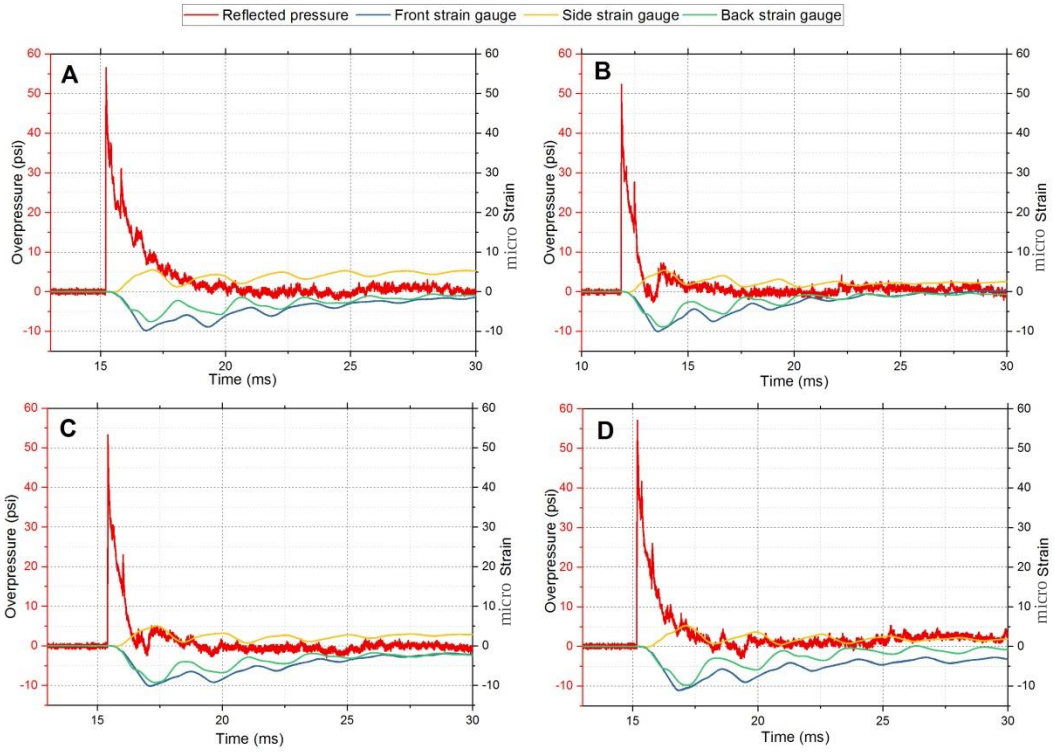

Figure 4.26 Time profiles of the strain gauges representing the tension and compression of the polycarbonate cylinder.

Note: The figure represents comparison of the strain gauge data during different cases:

A. DI water without bubbles B. 50% glycerol solution without bubbles
C. DI water with bubbles D. 50% glycerol solution with bubbles

Similar to the observation in 70 kPa, the strain gauges represent the tension and compression of the polycarbonate wall impacted by shock wave in all different conditions irrespective of what medium is inside.

The arrival times of the strain gauges are compared in figure 4.27. Similar to the observation made in tests performed at 70kPa intensity, it is seen that the side strain gauge lags substantially and the response of the front and back strain gauge is close to each other.

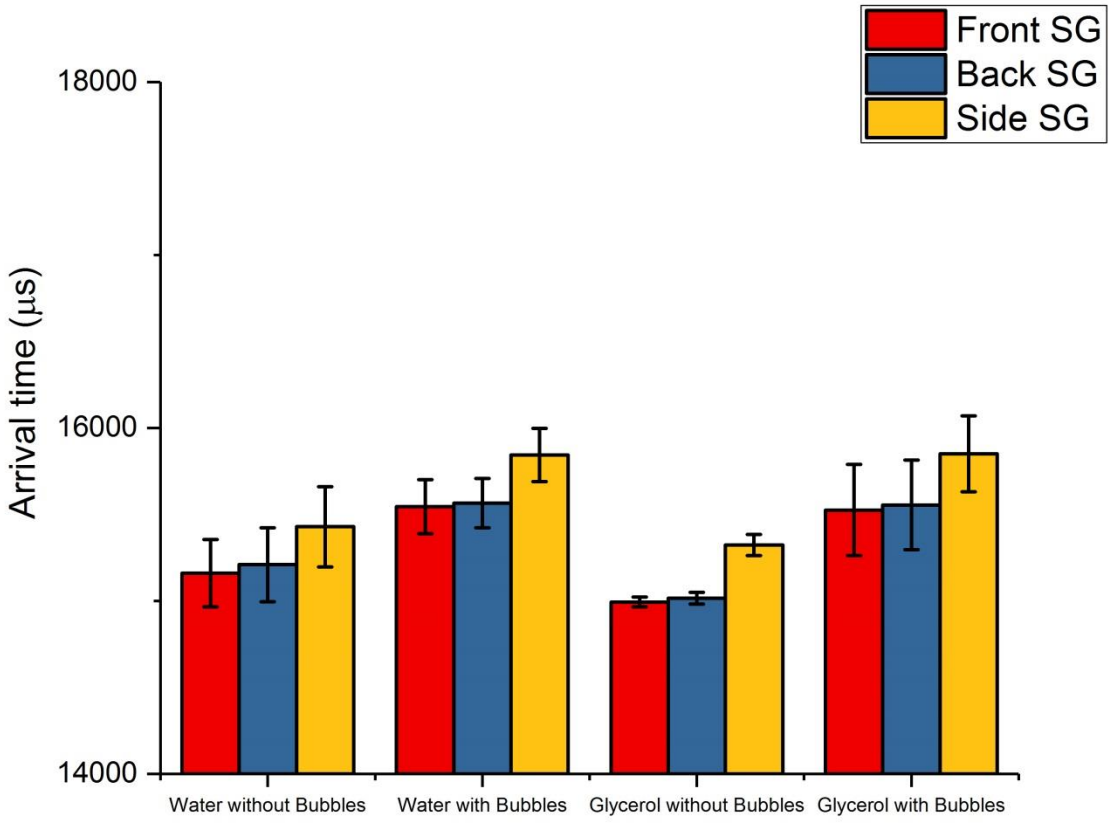

Figure 4.27 Comparison of arrival times for strain gauges at different locations.

4.4 Bubble Rupture – Comparing 70 kPa vs 130 kPa

It has been observed that more number of microbubbles are formed during bubble rupture, when the intensity of the shockwave is increased.

When observed under the same magnification, it can be qualitatively seen that more number of microbubbles are formed at 130 kPa shock intensity compared to 70 kPa shockwave intensity.

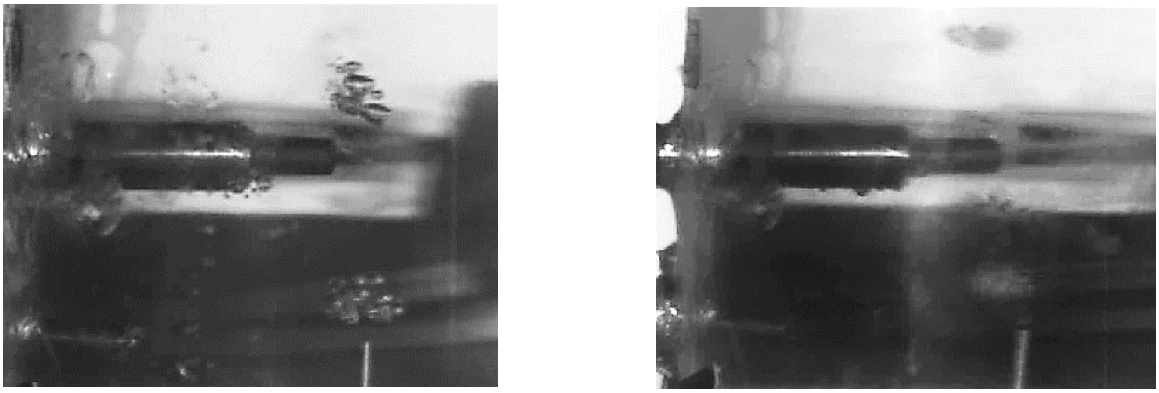

Figure 4.28 Comparison of bubble rupture in DI water at two different intensities.
Note: Left – DI water at 70 kPa shockwave intensity; Right – DI water at 130 kPa shockwave intensity

CHAPTER 5

CONCLUSION AND SUMMARY

The primary goal of this project is to investigate the effect of air bubbles introduction into the fluid on pressure response inside 2 inch diameter cylinder exposed to the shock waves. Polycarbonate cylinder is representative of human skull material and the medium inside, DI water and 50% glycerol-water solutions represent CSF and cerebral blood, respectively. The cylinder is exposed to different blast load conditions with incident pressures of 70 and 130 kPa.

The cylinder is allowed to move freely in one direction up to a certain point in order to better simulate the free field conditions.

Bubbles are created in a controlled manner to observe their behavior under shock loading conditions. It has been observed that high frequency bands have higher amplitude in pressure profiles recorded by the sensors indicative of bubble rupture.

Top sensor, which is close to the bubble-rupture region, shows high variation in both the fluids (DI water and 50% glycerol-water solution) at both the intensities (70 kPa and 130 kPa). This indicates that the bubble rupture contributes to the variation in the peak pressures in the fluid.

Also, when the peak pressure values in the sensors are compared in 70 kPa with 130 kPa, higher peak is observed when the polycarbonate cylinder is exposed to 130 kPa with the peak values almost twice that of the peak values observed at 70 kPa.

5.1 Limitations

Although the results from the experiments offer some insight into the effect associated with bubble presence in the media, there are some limitations of this study that need to be considered:

1. The cylinder selected for this study is made up of polycarbonate as which has acoustic properties close to that of bone material:- but the geometry of the skull is extremely different.

2. The skull does not have uniform thickness throughout like the cylinder. The human skull varies in thickness from 4 mm to 8 mm, while in our experiments uniform wall thickness polycarbonate cylinder is used. The geometry has been simplified for convenience of performing the experiment.

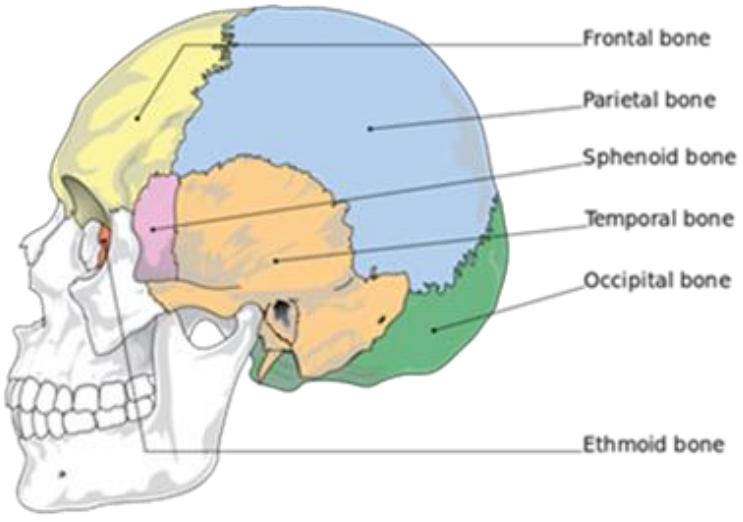

Figure 5.1 Side-view of cranial bones of skull
Source: (Troy)

Table 5.1 Skull Thickness at Different Bones
Source: (J.Baer and E.Harris)

Skull bone	Thickness (mm)
Frontal	7
Temporal	4
Occipital	6
Parietal	8

Cylinder of only one thickness (1.9 mm) is used to conduct the experiments. Experiments with one uniform thickness cannot predict the deformation and strain response of the skull.

3. When an object is subjected to blast, many reflections take place which are not considered for this thesis work, as the main purpose of this study is to look into the pressure change in the fluid due to the bubble rupture during blast loading conditions.

4. The size of the bubbles is much bigger than in real-life scenario. As we needed to observe controlled and continuous bubbles in the polycarbonate cylinder and view them visually through the video camera during the shock loading conditions, the size of the bubbles is bigger. In ideal scenario, the bubbles produced during cavitation are microscale bubbles(Haniff et al.).

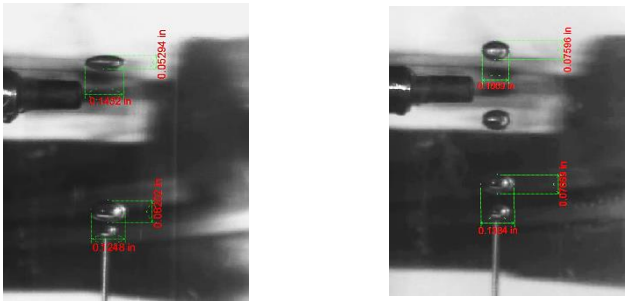

Figure 5.2 Size of the bubbles generated.
Note: measurements done in different fluids; left-DI water and right-50% glycerol-water solution

ProAnalyst software is used to quantify the size of the bubbles generated in different medium (DI water and 50% glycerol-water solution). The height and width of the bubbles was measured (N=30) using the cylinder diameter as the calibration factor (2 inches).

Table 5.2 Size of the Bubbles Measured

Medium	Width		Height	
	Average	SD (N=30)	Average	SD (N=30)
DI water	0.127 inch (3.22 mm)	0.01 inch (0.25 mm)	0.096 inch (2.43 mm)	0.11 inch (2.79 mm)
50% glycerol-water solution	0.119 inch (3.02 mm)	0.009 inch (0.22 mm)	0.081 inch (2.05 mm)	0.009 inch (0.22 mm)

5. The position of the bubble during the shock loading condition is not consistent all the time. It is close to the sensor at some instances and is away from the sensor at a few instances. The instant at which the shock wave occurs is not in our control and the position of the bubbles also varies with time, it is one of the major technical limitations affecting the pressure reading.

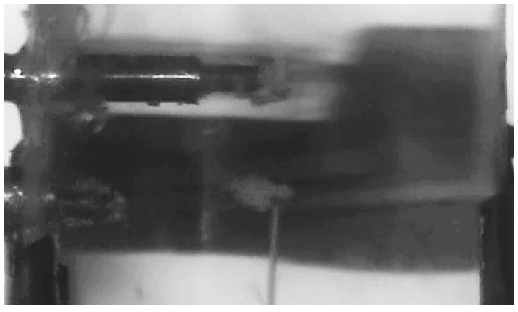

Figure 5.3 Bubble rupture close to the top sensor.

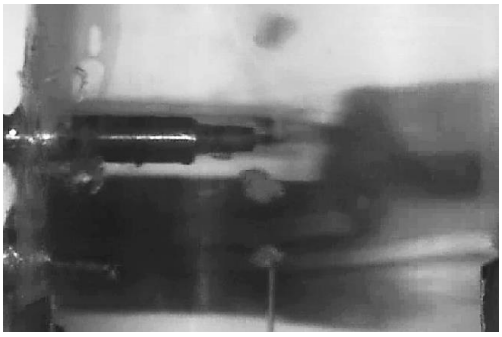

Figure 5.4 Bubble rupture away from the top sensor.

There is also some variation seen in the pressure profiles of the sensors when the bubble rupture takes place in different positions.

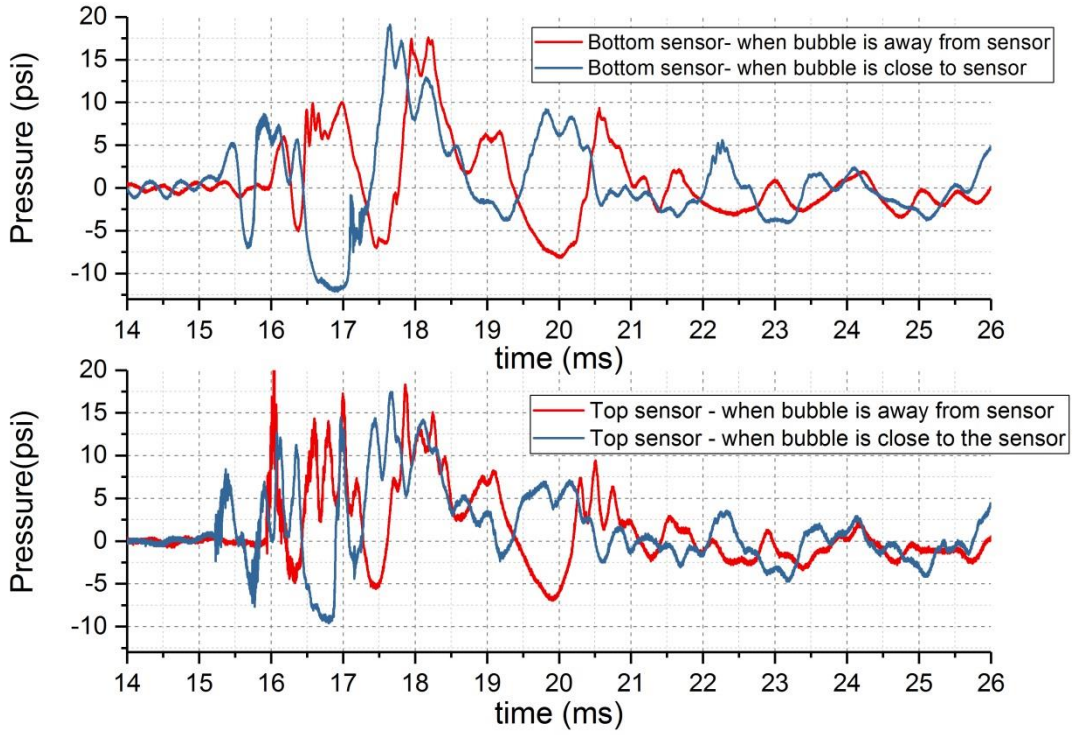

Figure 5.5 Pressure plots of the sensors when bubble ruptures at different positions with respect to the sensor.

It is seen that there are more negative peaks present in case where the bubble rupture is close to the sensor. Although, it is difficult to draw conclusions from these limited

experiments as the position of the bubbles with respect to the sensor during the shock-loading conditions was not repeatable and consistent in all cases.

6. The idealized skull-brain complex is a very simplified representation of the complex skull and brain model. The medium used inside the polycarbonate is chosen to be a homogenous single material at a time for doing the experiments which does not typically represent the skull-CSF-brain complex completely.

5.2 Future Scope

1. Polycarbonate cylinder of only one thickness with one diameter is used to conduct the experiments. Cylinders of different thickness and different diameters can be used to study the variation of the pressure response in the fluid.

2. In this study, we find pressure variation in the fluid with and without bubbles, which implies that there are pressure changes when the bubbles rupture. But there is still not enough evidence that the bubble rupture causes damage to the brain. As a future work to this study, biological matter like neurons can be cultured to find if these bubble rupture actually have the potential to damage the neurons and cause injury or not.

3. All the tests in this study are done experimentally. They can be further simulated and verified using software like ABACUS© or ANSYS©.

REFERENCES

Cernak, I., and L. J. Noble-Haeusslein. "Traumatic Brain Injury: An Overview of Pathobiology with Emphasis on Military Populations." *Journal of Cerebral Blood Flow and Metabolism* 30.2 (2010): 255-66. Print.

E.Brennen, Christopher. "Cavitation in Bioengineering Contextx." *Fifth International Symposium on Cavitation (cav2003) Osaka, Japan, November 1-4, 2003*. 2003. Print.

Goeller, J., et al. "Investigation of Cavitation as a Possible Damage Mechanism in Blast-Induced Traumatic Brain Injury." *Journal of Neurotrauma* 29.10 (2012): 1970-81. Print.

Haniff, S., et al. *Virtual Simulation of the Effects of Intracranial Fluid Cavitation in Blast-Induced Traumatic Brain Injury*. Proceedings of the Asme International Mechanical Engineering Congress and Exposition, 2015, Vol 3. New York: Amer Soc Mechanical Engineers, 2016. Print.

J.Baer, Melvyn, and James E.Harris. *A Commentary on the Growth of the Human Brain and Skull*. Vol., 1969. 39-44. Web.

The Shape of the Blast Wave: Studies of the Friedlander Equation. 21st International Symposium on Military and Blast, Israel. 2010. Print.

K.Gupta, Raj, and Andrzej Przekwas. "Mathematical Models of Blast-Induced Tbi: Current Status, Challenges and Prospects." *Frontiers in Neurology* 4 (2013). Print.

Kuriakose, M., et al. "Tailoring the Blast Exposure Conditions in the Shock Tube for Generating Pure, Primary Shock Waves: The End Plate Facilitates Elimination of Secondary Loading of the Specimen." *Plos One* 11.9 (2016): 19. Print.

Miner;, C. S., and N. N. Dalton. *Physical Properties of Glycerine and Its Solutions*. Hydrocarbon Processing: Gulf Publishing Company, May 1967. Print.

Neumann;, and John von. *The Point Source Solution*. Ed. A.J.Taub. Vol. 61963. Print.

R.S.Salzar, et al. "Experimental Investigation of Cavitation as a Possible Damage Mechanism in Blast-Induced Traumatic Brain Injury in Post-Mortem Human Subject Heads." *Journal of Neurotrauma* (2016). Print.

Santner, Dr. Friedrich. "Viscopedia | a Free Encyclopedia for Viscosity." *Whole blood*. Limited Liability company. Web.

Selvan, V., et al. "Blast Wave Loading Pathways in Heterogeneous Material Systems-Experimental and Numerical Approaches." *Journal of Biomechanical Engineering-Transactions of the Asme* 135.6 (2013). Print.

Sundaramurthy, A., and N. Chandra. "A Parametric Approach to Shape Field-Relevant Blast Wave Profiles in Compressed-Gas-Driven Shock Tube." *Frontiers in Neurology* 5 (2014): 10. Print.

Troy, Eric. "Bones of the Adult Skeleton Part One: The Axial Skeleton." (2012). Web.